TECHNICAL REPORT

ISO/TR 23173

First edition
2021-06

Surface chemical analysis — Electron spectroscopies — Measurement of the thickness and composition of nanoparticle coatings

Analyse chimique des surfaces — Spectroscopies d'électrons — Mesurage de l'épaisseur et de la composition des revêtements de nanoparticules

Reference number
ISO/TR 23173:2021(E)

ISO copyright office
CP 401 • Ch. de Blandonnet 8
CH-1214 Vernier, Geneva
Phone: +41 22 749 01 11
Email: copyright@iso.org
Website: www.iso.org

Published in Switzerland

Contents

Page

Foreword

ISO (the International Organization for Standardization) is a worldwide federation of national standards bodies (ISO member bodies). The work of preparing International Standards is normally carried out through ISO technical committees. Each member body interested in a subject for which a technical committee has been established has the right to be represented on that committee. International organizations, governmental and non-governmental, in liaison with ISO, also take part in the work. ISO collaborates closely with the International Electrotechnical Commission (IEC) on all matters of electrotechnical standardization.

The procedures used to develop this document and those intended for its further maintenance are described in the ISO/IEC Directives, Part 1. In particular, the different approval criteria needed for the different types of ISO documents should be noted. This document was drafted in accordance with the editorial rules of the ISO/IEC Directives, Part 2 (see www.iso.org/directives).

Attention is drawn to the possibility that some of the elements of this document may be the subject of patent rights. ISO shall not be held responsible for identifying any or all such patent rights. Details of any patent rights identified during the development of the document will be in the Introduction and/or on the ISO list of patent declarations received (see www.iso.org/patents).

Any trade name used in this document is information given for the convenience of users and does not constitute an endorsement.

For an explanation of the voluntary nature of standards, the meaning of ISO specific terms and expressions related to conformity assessment, as well as information about ISO's adherence to the World Trade Organization (WTO) principles in the Technical Barriers to Trade (TBT), see www.iso.org/iso/foreword.html.

This document was prepared by Technical Committee ISO/TC 201, *Surface chemical analysis*, Subcommittee SC 7, *Electron spectroscopies*.

Any feedback or questions on this document should be directed to the user's national standards body. A complete listing of these bodies can be found at www.iso.org/members.html.

Introduction

Recently, there has been increasing development and use of nanoparticles in a wide range of application areas, including catalysis, medicine, energy, optoelectronics and cosmetics[1]–[7]. In particular, nanoparticles having some form of coating layer, which is present either by design or due to incidental processes such as contamination or oxidation, are among the most commonly studied and utilised[8]–[11]. An essential part of the characterisation of nanoparticles is the measurement of the surface properties because a large proportion of the material is at a surface or interface. In the case of coated nanoparticles, the thickness and composition of the coating has a significant role determining its functional properties and defines the interaction of the particle with its environment. Many applications require nanoparticles to have coatings that are specifically designed in order to achieve a desired level of performance. Measurement of surface composition and coating thickness of nanoparticles is a challenge to which electron spectroscopies are well suited, due to high surface sensitivity, well-understood physical principles and accessibility. Such measurements can have a significant dependence on sample format and condition; sample handling and provenance of nanoparticle samples for surface chemical analysis are addressed in ISO 20579[12]. A general introduction to the challenges of surface chemical analysis of nanostructured materials is provided in ISO/TR 14187[13].

Surface chemical analysis — Electron spectroscopies — Measurement of the thickness and composition of nanoparticle coatings

1 Scope

This document provides a description of methods by which the coating thickness and chemical composition of "core-shell" nanoparticles (including some variant and non-ideal morphologies) can be determined using electron spectroscopy techniques. It identifies the assumptions, challenges, and uncertainties associated with each method. It also describes protocols and issues for the general analysis of nanoparticle samples using electron spectroscopies, specifically in relation to their importance for measurements of coating thicknesses.

This document focuses on the use of electron spectroscopy techniques, specifically X-ray photoelectron spectroscopy, Auger electron spectroscopy, and synchrotron-based methods. These cannot provide all of the information necessary for accurate analysis and therefore some additional analytical methods are outlined in the context of their ability to aid in the interpretation of electron spectroscopy data.

2 Normative references

The following documents are referred to in the text in such a way that some or all of their content constitutes requirements of this document. For dated references, only the edition cited applies. For undated references, the latest edition of the referenced document (including any amendments) applies.

ISO 18115-1, *Surface chemical analysis — Vocabulary — Part 1: General terms and terms used in spectroscopy*

ISO 18115-2, *Surface chemical analysis — Vocabulary — Part 2: Terms used in scanning-probe microscopy*

3 Terms and definitions

For the purposes of this document, the terms and definitions given in ISO 18115-1 and ISO 18115-2 apply.

ISO and IEC maintain terminological databases for use in standardization at the following addresses:

— ISO Online browsing platform: available at https://www.iso.org/obp

— IEC Electropedia: available at https://www.electropedia.org/

4 Symbols and abbreviated terms

X subscripts	denote the material of the overlayer
Y subscripts	denote the material of the core
x subscripts	denote a specific photoelectron peak from material *X*
y subscripts	denote a specific photoelectron peak from material *Y*
I_i	intensity of electrons arising from a peak, *i*

$I_{i,I}$	intensity of electrons from peak i arising from pure material I
a	vertical thickness of the overlayer material at a given position
b	vertical thickness of the core material at a given position
$L_{i,J}$	effective attenuation length of electrons from peak i travelling through material J
R	nanoparticle core radius
T	thickness of the overlayer
d	horizontal displacement of a specific line of material
θ	angle between the central vertical axis of the particle and the point of the particle's surface which is at displacement x
$A_{x,y}$	normalised intensity ratio of the intensities of peaks x and y
γ	dimensionless scaling factor
T_∞	estimated overlayer thickness for a large sphere
T_0	estimated overlayer thickness for infinitesimally small particles
T_{NP}	estimated overlayer thickness for a nanoparticle
AES	Auger electron spectroscopy
AFM	atomic force microscopy
CSNP	core-shell nanoparticle
EAL	effective attenuation length
EDX	energy dispersive X-ray analysis
ICP-AES	inductively coupled plasma atomic emission spectroscopy
IMFP	inelastic mean free path
KE	kinetic energy
MPA	mercaptopropanoic acid
NAP-XPS	near-ambient-pressure x-ray photoelectron spectroscopy
NP	nanoparticle
SAM	scanning Auger microscopy
SANS	small angle neutron scattering
SAXS	small-angle X-ray scattering
SEM	scanning electron microscopy
TEM	transmission electron microscopy

TOP	trioctylphosphine
UHV	ultra-high vacuum
XPS	X-ray photoelectron spectroscopy

5 Overview

The methods described in this document are listed by clause and outlined in Table 1. The primary use detailed is the determination of the thickness of a nanoparticle coating from electron spectroscopy data, for which three main methods are described, with a specific example given for each. Methods for coating thickness determination that are described in detail include the use of descriptive formulae for calculation of coating thicknesses from X-ray photoelectron spectroscopy (XPS) peak intensities; numerical modelling of XPS intensities from nanoparticles, and general structure and layer thickness determination by the use of in-depth simulation software. Interpretation of sample composition from electron spectroscopy data for layered samples is discussed. Rudimentary analysis of the inelastic background in XPS data is described, alongside the relevant considerations for interpreting inelastic backgrounds from nanoparticle samples. Discussions of the use and potential benefits of synchrotron-XPS, near-ambient-pressure XPS (NAP-XPS), and Auger electron spectroscopy (AES) are included, along with any related issues and considerations. For all methods of analysis, additional characterisation is required before confident estimates of coating thickness or composition can be made. Therefore, a range of measurement techniques which are complementary to electron spectroscopy analysis, the benefits they provide, and any relevant concerns or disadvantages are outlined. A number of alternate morphologies and deviations from a uniform concentric core-shell structure are described. The effects these structural variations have on data from such samples are identified, and methods for their interpretation and analysis are discussed.

Table 1 — Summary of methods and analyses outlined in this document for the measurement of the thickness and composition of nanoparticle coatings

Clause	Details
6.4 Numerical methods	The use of simple numerical modelling to generate estimated XPS peak intensities from nanoparticles of a defined morphology. A method by which such modelling can be performed is provided, alongside a simple MathWorks® MATLAB script for performing such calculations.
6.5 Descriptive formulae	The use of methods for calculation of overlayer thicknesses using empirical or semi-empirical formulae derived from theory or modelling. Typically, these are methods whereby measured data can be input directly into a set of equations in order to derive a single calculated coating thickness value.
6.6 Modelling and simulation software	The use of electron spectroscopy modelling and simulation software. SESSA is described in detail as an example, and comparisons between it and the other methods herein are summarised, with examples.
6.8 Inelastic background analysis	Overview of the analysis of the inelastic background signal in XPS for planar overlayers, and the potential application of this for coated nanoparticles.
6.9 Elemental composition	Overview of the extraction of elemental compositions from electron spectroscopy data for coated nanoparticles And the challenges posed by systems with internal structure.
6.10 Variable excitation energy XPS	The use of variable-photon-energy XPS (e.g. utilising a synchrotron light source) for depth profiling of nanoparticles. The capabilities and applications of such methods are described, with examples.
6.11 Near-ambient-pressure XPS (NAPXPS)	An outline of the use of NAPXPS to coated nanoparticle systems, specifically regarding the potential differences between samples analysed in ultra-high vacuum conditions compared to those in an environment relevant to their application.

Table 1 *(continued)*

Clause	Details
Clause 7 Auger Electron Spectroscopy (AES)	A summary of Auger electron spectroscopy for the analysis of nanoparticles, including destructive and non-destructive depth profiling, imaging, and line-scans of individual particles. Several examples of use are summarised.
Clause 8 Complementary techniques	A list of supporting measurement techniques which provide information that can be useful when analysing electron spectroscopy data from nanoparticles. The benefits and disadvantages of each suggested technique are outlined.
Clause 9 Deviations from ideality	A summary of how nanoparticle systems might deviate from the idealised model of a uniform, concentric, spherical coated nanoparticle, and the effects of such deviations on electron spectroscopy data.

6 X-ray photoelectron spectroscopy

6.1 General

XPS provides quantitative information of the surface composition of a sample by the collection of photoelectrons emitted under exposure to an x-ray beam. The information depth of XPS is limited by the attenuation of the electrons through the sample, which itself is determined by both the properties of the sample material, and the kinetic energy of the emitted electrons. Lab-based instruments typically use either aluminium or magnesium K_α x-rays at a photon energy of 1 486,6 eV or 1 253,6 eV, respectively, this corresponds to a maximum information depth for the elastic photoelectron peaks of approximately 10 nm. More recently, lab-based instruments with higher energy X-ray sources have also been developed, with correspondingly larger information depths due to the higher kinetic energies of the photoelectrons.

Due to this high surface sensitivity, XPS is an inherently nanoscale technique in terms of depth of analysis and is thus suited to the analysis and characterisation of nano-objects. It is commonly used to provide quantitative information on the relative concentrations of elements within the surface of a sample under the assumption of homogeneity, however with a proper understanding of the underlying theory and appropriate methodology, greater information on the surface structure of samples can be extracted.

In most lab-based XPS instruments, the analysis area under standard operating conditions is on the order of 0,01 mm^2 to 1 mm^2 with some instruments possessing lens-based area-limiting or micro-focussed x-ray beams that allow analysis areas down to 10^{-4} mm^2; thus for samples of nanomaterials XPS typically serves as a population measurement technique, where the measured intensities are an average of the material within the analysis area.

Given the high surface sensitivity of XPS, it is also of crucial importance that samples be prepared, handled, and cleaned with appropriate procedures. The presence of contaminants within a sample can drastically influence the results of any measurements made. This is of especial importance for nanomaterial samples, which may often require more careful preparation, or be susceptible to additional sources of contamination. ISO 20579-4 discusses the issues relating to the handling of nano-objects prior to surface analysis[12].

6.2 Coating thickness measurement

For flat, uniform surfaces measurement of overlayer thickness using XPS has been understood for some time. A formula for the calculation of oxide overlayer thicknesses was developed in the 1970s[14]. More recently, ISO 14701[15],dealing with the measurement of silicon oxide thickness using XPS, has been published. For reporting on measurements of overlayer thicknesses using XPS, ISO 13424[16] describes the information to be included. For cases where the overlayer and substrate peaks to be quantified are not of similar kinetic energy, a graphical method known as the "Thickogram"[17] was developed. In any

calculation of an overlayer thickness, it is necessary that the peak areas corresponding to the overlayer and substrate materials are identifiable and measurable.

For samples which are not flat, such methods will be in error due to the effects of sample geometry on the path-length of electrons through the overlayer. Under the assumption of a uniform overlayer thickness, a sample with a flat surface oriented for normal emission to the detector presents the shortest possible direct path for electrons through the overlayer. For a conformal, uniform overlayer any topography therefore increases this path length, in a manner equivalent to tilting the sample. Analytical methods to determine the "effective average tilt" of the sample which results from the topography[18] have been developed if the topography is either known or can be measured, for example by atomic force microscopy (AFM). For generic morphologies such as spheres and cylinders, a simpler method using the concept of "topofactors" has been shown[19]. In methods of this type, a calculation is made treating the sample as if flat, and then the relevant "topofactor" is applied to correct for the known topography[19]–[21].

Such methods for measurement of overlayers on topographic samples apply only in the case where the topography is on the macroscopic scale – that is, they cannot account for topography on the scale of the electron IMFP's within the material. At this length scale the volumetric contribution of the coating to the XPS data becomes significant and the assumption of a continuous underlying substrate becomes invalid. For nanoparticle samples, the presence of overlayer material on the sides and underside of the particles, and potentially even particles beneath the outermost layer, can contribute to the measurement result.

6.3 Nanoparticle coating thickness

Several methods for the determination of nanoparticle coating thicknesses from XPS data are available. These can broadly be categorised into three types: simple numerical modelling, empirically determined formulae and the use of more rigorous simulation software. When any analysis of XPS data from nanoparticles is considered however, there are several assumptions which are typically made. Hereafter, particles conforming to these assumptions are described as "ideal" core-shell particles.

— The analysis area is assumed to be representative of the whole sample, exhibiting no macroscopic variation. In situations where this is not the case, multiple non-overlapping analysis areas can be used to assess the effect of any variation.

— Unless specifically accounted for, the nanoparticles are assumed to be randomly deposited, with no large-scale ordering[22]. This assumption is not necessary if the analysis method requires, or is capable of modelling, particles in a specific distribution.

— All of the measured XPS peak intensities are assumed to arise from the nanoparticles, with no significant contribution from the substrate or contaminants[10].

— The core material and coating are each assumed to be uniform in density, i.e. possess no gaps, density gradients, or similar. It follows from this assumption that the boundary between the core and coating materials is abrupt, with no mixing layer.

— The core and coating are assumed to form a pair of concentric spheres.

— All the particles in the analysed population are identical in both chemical and physical structure.

— There is no significant contribution to the signal from particles below the outermost layer, i.e. the electron path lengths do not exceed the particle size.

Depending on the analysis method selected, some of these assumptions might not be necessary, or deviations can be accounted for. This is particularly true for more advanced simulation methods, as these can be capable of accounting for many possible structural variations. Because there are a large number of possible structural variations which are indistinguishable directly from XPS data, it is important that deviations from the typical assumed case are understood and characterised using relevant analytical techniques. In some cases, variation in the XPS measurements taken can be used to corroborate or disprove these assumptions; for example the use of multiple separate analysis areas to judge sample homogeneity. Sample rotation (with respect to the analyser) may be used to identify

the presence, or lack, of signal arising from the substrate, or to indicate structural discrepancies; for spherical, randomly deposited particles, angle-dependant XPS should not observe differences in the relative signal observed from the core and shell. Any discrepancy would therefore be due either to signal from the substrate, or structural deviations.

In most realistic scenarios, many of these assumptions are invalid to some degree. The effects of deviations from the assumed morphology are discussed in Clause 9.

6.4 Numerical methods

In general, a numerical modelling approach involves writing a simple script or program to calculate relative XPS intensities for the core and overlayer materials arising from a nanoparticle. By performing such calculations programmatically, for a large array of core/shell sizes, and then comparing to experimental data, an estimate of overlayer thickness can be made. Numerical modelling of the attenuation of electrons through material can be used in order to generate expected XPS peak intensities for any given material and can be applied to a broad range of sample morphologies. Despite this, there are relatively few examples of numerical modelling in the literature[23]–[25]. An understanding of the attenuation of electrons through material is required in order to correctly apply this method; this information can be readily found throughout the literature[14],[17],[19],[22]–[25]. Likewise, a rudimentary understanding of the relevant geometrical calculations is necessary, particularly if non-ideal morphologies are being considered.

Numerical modelling of this type can be performed using a broad range of software. Scientific scripting environments such as MATLAB are ideally suited, however the procedure can be translated to the majority of common programming languages and is simple enough to be implemented within common spreadsheet manipulation software. It is suited for use with most types of nanoparticle system and is particularly beneficial for systems which cannot be resolved using any descriptive formula, but which still possess a well-understood geometry.

Typically, the first step in using numerical modelling involves calculating the relative XPS intensities for the core and overlayer materials arising from a vertical line through the particle. The signal from this line can be considered equivalent to a stack of planar overlayers. The effects of elastic scattering can be corrected for by the use of effective attenuation lengths (EALs) in calculations of electron attenuation through the material. In this case, the intensities for the core and overlayer materials arising from a single line of material within an ideal particle are given by Formulae (1) and (2):

$$I_x = I_{x,X}\left[1-e^{\left(\frac{-a}{L_{x,X}}\right)}\left(1-e^{\left(\frac{-b}{L_{x,Y}}\right)}\left(1-e^{\left(\frac{-a}{L_{x,X}}\right)}\right)\right)\right] \tag{1}$$

$$I_y = I_{y,Y}e^{\left(\frac{-a}{L_{y,X}}\right)}\left(1-e^{\left(\frac{-b}{L_{y,Y}}\right)}\right) \tag{2}$$

where

X, Y are the materials of the overlayer and core, respectively;

x and y are the specific photoelectron peaks from materials X and Y;

I_i is the intensity of electrons arising from a peak, i;

$I_{i,I}$ is the intensity of electrons from peak i arising from pure material I;

a is the vertical thickness of the overlayer material at a given position;

b is the vertical thickness of the core material at a given position;

$L_{i,J}$ is the effective attenuation length of electrons from peak, i, travelling through material J.

For lines which do not pass through the core, where b=0, Formulae (1) and (2) are still valid. For situations in which one of the elements within a sample is present within both the core and overlayer, simply summing the outputs of both equations will provide the total intensity for that element.

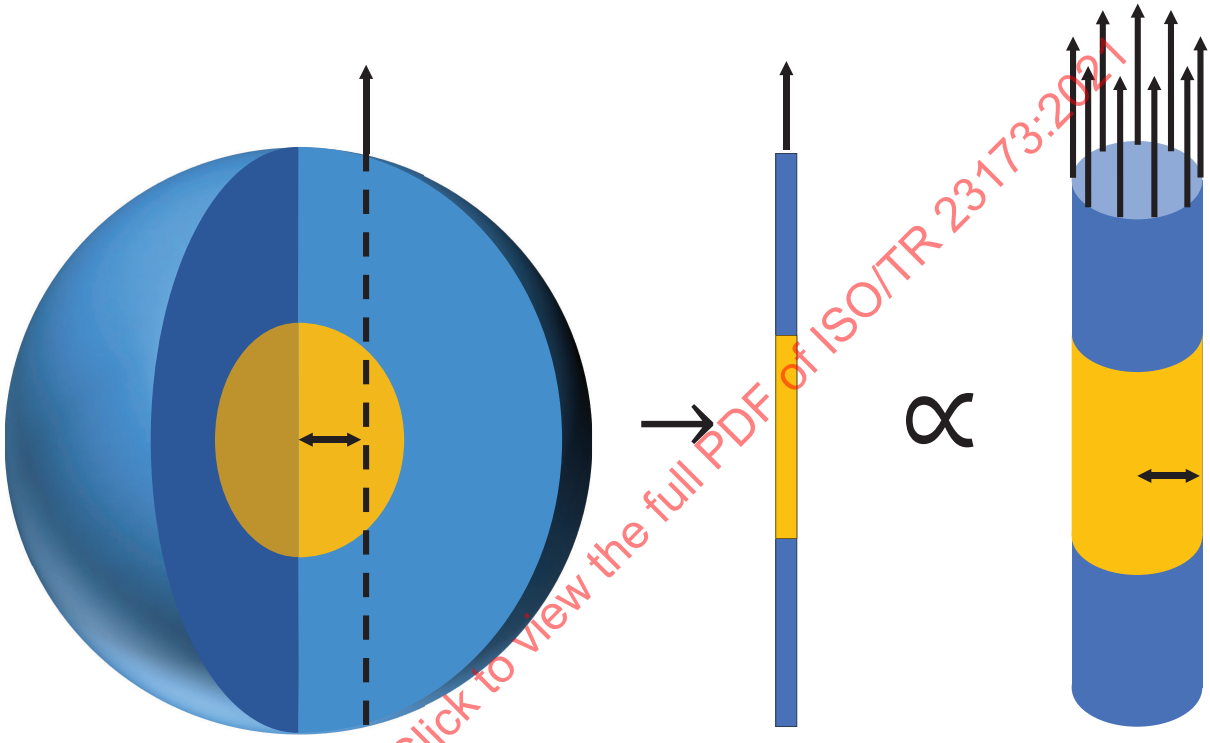

Figure 1 — Schematic illustration of the equivalence of the XPS intensity observed from an infinitesimal line at a fixed horizontal displacement to that of the hollow cylinder describing all lines at identical horizontal displacement

This calculation is repeated for an array of parallel lines through the particle and the intensities for each line summed across the entire geometry of the particle with appropriate weighting for the area represented by each line. For spherically symmetrical particles, the relative intensities arising from a vertical line of material are equivalent to those originating from the hollow cylinder described by the rotation of this line around the central vertical axis of the particle, as shown in Figure 1. Therefore, the calculation reduces to a one-dimensional summation of displacements from the central axis of the particle, with correction factors applied to account for the differing circumferences of the cylinders.

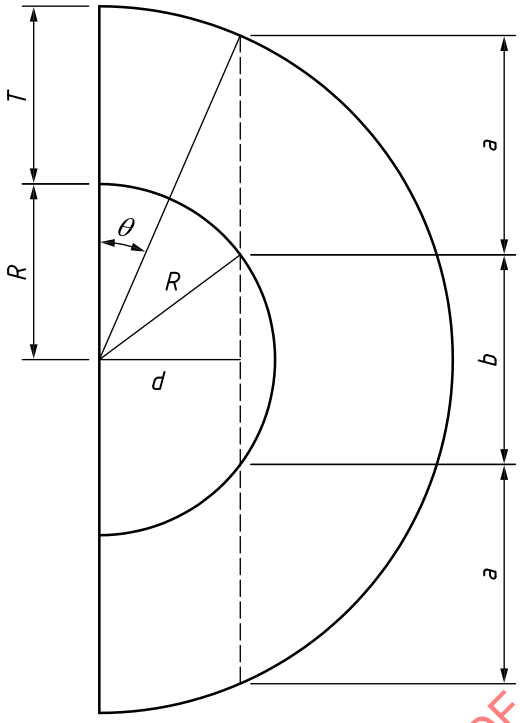

Figure 2 — Schematic of the geometry relevant to calculation of intensities from a specific line of material at a horizontal displacement x from the central vertical axis of the particle

Figure 2 depicts the relevant geometry for calculating the dimensions of an individual line of material, It is most efficient to perform the intensity calculations given in Formulae (1) and (2) in a loop from $\theta = 0$ rad to $\theta = \frac{\pi}{2}$ rad. Using this method, the parameters in Figure 2 are related by Formulae (3) to (6).

$$d = (R+T)\sin\theta \tag{3}$$

$$2a + b = 2(R+T)\cos\theta \tag{4}$$

$$b = \begin{cases} 2\sqrt{R^2 - d^2}, d < R \\ 0, d > R \end{cases} \tag{5}$$

$$a = (R+T)\cos\theta - b/2 \tag{6}$$

where

R is the nanoparticle core radius;

T is the thickness of the overlayer;

d is the horizontal displacement of a specific line of material;

a is the vertical thickness of the overlayer at displacement d;

b is the vertical thickness of the core at displacement d;

θ is the angle between the central vertical axis of the particle and the point of the particle's surface which is at displacement d.

If performing the geometry summation in this way (i.e. summing for a range of values of θ) two correction factors need to be applied. Firstly, the intensities from each individual line will be equivalent

to those from a hollow cylinder of variable radius. The intensity sum therefore needs to be corrected for the increasing circumference with increasing d. The circumference is linearly proportional to d', and thus from Formula (3), to $sin\theta$. Secondly, a correction is applied to account for the variation in thickness of each hollow cylinder, which is equivalent to the differential change in d, d'. As d is proportional to $sin\theta$, d varies as $cos\theta$. Thus, with both corrections applied, the intensities for each line need to be multiplied by a factor of $sin\theta cos\theta$.

An example MATLAB script with commentary explaining the steps is given in Annex A.

This method can be used to generate accurate estimates of overlayer thickness by performing the calculation over a range of overlayer thicknesses, plotting the resulting intensity ratio, and comparing to experimentally observed values. Typically the most significant contributor to the uncertainty is the ~10 % uncertainty in the estimation of effective attenuation lengths[24],[26]. The method assumes a straight-line trajectory for all detected electrons, i.e. elastic scattering is corrected for by the use of EALs. For nanoparticles with organic or low-Z element overlayer materials, this assumption is reasonably valid. However, for high-Z overlayers, the effect of elastic scattering can become significant.

This method can be extended to cover non-ideal nanoparticle systems such as those with a non-central core, or significant polydispersity. In such cases it is important to have an otherwise complete characterisation of the particles. For example, in the case of a non-central core, the diameters of both the core and the complete particle are required to estimate the displacement of the core. Likewise, if quantification of the amount of overlayer material for such a system was needed, core diameter and displacement would be required. In all such cases of particle asymmetry, the distribution of nanoparticle orientations within the sample deposit is also required and any ordering with respect to the asymmetry will need to be accounted for. In all cases except fully aligned particles, the full range of particle orientations will need to be calculated with appropriate geometric weightings.

6.5 Descriptive formulae

The most accessible method to enable the general XPS analyst to efficiently estimate overlayer thicknesses is through the use of descriptive formulae[23],[24],[27], for which the only expertise required is moderate mathematical literacy. Typically, such methods are either developed by empirically or semi-empirically fitting data obtained from a more complex modelling or a simulation-based approach[24], or in some more constrained conditions, approximate analytical formulae have been derived[28]. The most well-known method in current use is the "T_{NP}" method[24]. This method can be applied simply by methodical application of the required formulae, which, for efficiency, can be readily encapsulated by a simple spreadsheet. The ease of use and repeatability of this method have been demonstrated through its application by many of the participants of an interlaboratory study into measurement of coating thicknesses[10].

The T_{NP} method for the determination of shell thicknesses of core-shell nanoparticles is an empirical method developed by comparison to numerical modelling, similar to that described previously in 6.4. Formulae for a distinct set of size regimes or limits were determined, and in combination are used to produce a general formula for estimation of overlayer thicknesses on nanoparticles. The resulting expression is encapsulated in Formulae (7) to (11), which are mathematically identical to those in the original work[24], but are slightly simplified.

$$A_{x,y} = \frac{I_x I_{y,Y}}{I_{x,X} I_y} \tag{7}$$

$$T_\infty = \frac{0{,}74 A_{x,y}^{3,6} \ln\left(A_{x,y}\right) L_{y,X}^{0,9} L_{x,X}^{0,1} + 4{,}2 A_{x,y} L_{y,X}^{0,41} L_{x,X}^{0,59}}{A_{x,y}^{3,6} + 8{,}9} \tag{8}$$

$$T_0 = R\left[\left(\frac{A_{x,y} L_{x,X}^2}{L_{y,X} L_{x,Y}} + 1\right)^{1/3} - 1\right] \tag{9}$$

$$\gamma = \frac{L_{y,X}^{0,5} L_{x,Y}^{0,4} L_{x,X}^{0,1}}{A_{x,y}^{0,1} R} \tag{10}$$

$$T_{NP} = \frac{T_\infty L_{x,X} + \left(\gamma^{3,5} + 0{,}565\gamma^{2,5}\right) R T_0}{(1+1{,}8\gamma) L_{x,X} + \left(\gamma^{3,5} + 0{,}565\gamma^{2,5}\right) R} \tag{11}$$

where

X and Y	are the materials of the shell and core, respectively;
x and y	are specific photoelectron peaks from materials X and Y;
$A_{x,y}$	is the normalised intensity ratio of the intensities of peaks x and y;
I_i	is the intensity of electrons from peak i;
$I_{i,I}$	is the intensity of electrons from peak i arising from pure material I;
$L_{i,J}$	is the effective attenuation length of electrons from peak i travelling through material J;
R	is the nanoparticle core radius;
γ	is a dimensionless scaling factor;
T_∞	is the estimated overlayer thickness for a large sphere;
T_0	is the estimated overlayer thickness for infinitesimally small particles;
T_{NP}	is the estimated overlayer thickness for a nanoparticle.

The information required is the particle core size, R, and the measured XPS peak intensities for the core, I_y, and overlayer, I_x. The measured relative intensity from pure reference materials of the core and the shell, $I_{y,Y}:I_{x,X}$ is also recommended, however in cases where this is difficult to obtain, estimated values can suffice. A step by step procedure for applying this method is given below.

a) Determine or retrieve values for the effective attenuation lengths $L_{i,J}$ [26],[29]–[31].

b) Measure I_x and I_y from XPS data.

c) Measure, or estimate, pure material intensities $I_{x,X}$ and $I_{y,Y}$.

d) Calculate $A_{x,y}$ from Formula (8).

e) Calculate T_0, T_∞, and γ using Formulae (8) to (10).

f) Determine T_{NP} using Formula (11).

The T_{NP} method encapsulates the straight-line-approximation for most ideal core-shell particles and compensates for the effects of elastic scattering by the use of EALs. Thus, the uncertainty in estimated overlayer thickness will be greatest for nanoparticle systems in which the coating is formed of high-Z elements or for which photoelectron peaks with relatively low energies are measured. The magnitude of elastic scattering effects can be usefully described using the albedo parameter detailed by Powell and Jablonski[32].

For the vast majority of practical cases, the uncertainty due to the use of this method will be less than the ~10 % uncertainty in the estimation of EALs[24],[26]. Figure 3 shows the distribution of thicknesses calculated by T_{NP}, for 10 000 randomly generated nanoparticles modelled using numerical methods as described previously within this document. Parameters for these particles were varied uniformly over the following ranges: core radii from 1 nm to 100 nm; overlayer thickness from 1 nm to 10 nm; electron kinetic energies (core or overlayer) from 200 eV to 1 400 eV; and Z_i values (core or overlayer) from

3-83. Within this regime, more than 80 % of the calculated overlayer thicknesses lie within ±10 % of the modelled value, and the standard deviation in the ratio of calculated to modelled thickness is ~8 %. It is worth noting that this dataset will contain a significant number of cases at the extremes of the physically plausible parameters which are unrepresentative of real particles.

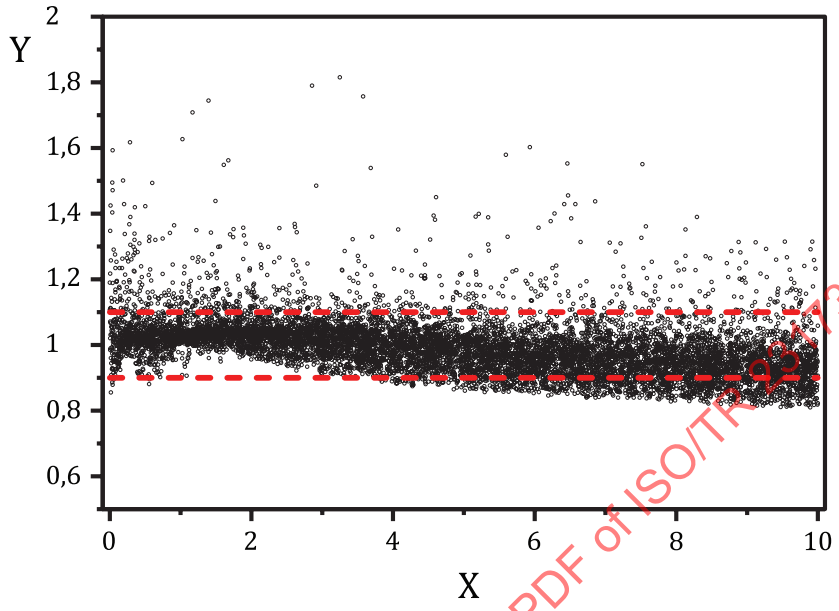

Key

X modelled overlayer thickness (nm)

Y ratio of calculated to modelled overlayer thickness

NOTE Dashed lines indicate ±10 % deviation from the modelled value. More than 80 % of the points fall within these lines.

Figure 3 — Plot of the ratio of the T_{NP} calculated overlayer thickness vs the thickness from the model, for 10 000 randomly generated nanoparticles

6.6 Modelling and simulation software

In some scenarios, descriptive formulae, or simple numerical modelling using the straight-line approximation can prove unsuitable. In situations where complex, varied morphologies are known to exist within a sample, numerical modelling can still be utilised, but will be quite arduous. In situations where elastic scattering can play a significant role, use of the straight-line approximation, and formulae based upon it, can become less accurate. To adequately interpret data from such systems, more in-depth simulations of electron transport and material properties are required. Software packages designed to allow the general analyst ready access to such simulations are available; the NIST database for the Simulation of Electron Spectra for Surface Analysis (SESSA) is currently one of the most well-known, and has been shown to be effective for the purpose of nanoparticle analysis[33]–[36].

SESSA itself contains databases for the majority of the parameters required for modelling electron spectroscopy data, (for example various interaction cross-sections, inelastic mean free paths, lineshapes) often from multiple sources including theoretical and empirical data. Many values can be adjusted by the user to fit their particular case, and all values are traceable to their literature source, with many including a statement concerning their reliability. This allows the user to determine for themselves their confidence in any given simulation result. The simulation itself is performed using Monte Carlo calculations based on the 'trajectory reversal' model in which electron trajectories are calculated backwards, originating in the detector; using this method improves the efficiency of simulation, as electron trajectories which do not contribute to the measured signal are not simulated[37],[38].

SESSA is capable of modelling a range of sample morphologies, ranging from simple planar structures, to more complex systems such as spheres, layered spheres, and islands. This allows the user whose samples are known not to meet the assumptions described previously for an ideal system, to reasonably estimate their structure. With any modelling process such as this, care needs to be taken that appropriate constraints based on prior knowledge of the system are implemented; it is entirely possible that multiple morphologies and compositions can give rise to very similar spectra. As such, a model using an incorrect description of the particle structure can still result in a good match to the observed experimental result.

6.7 Method comparisons

For coated nanoparticle systems, several comparisons between SESSA simulations, empirical data, and other overlayer quantification methods have been reported[25],[33],[34],[39],[40]. Comparisons to both numerical modelling and the T_{NP} method discussed in this document have shown good agreement between all three methods. Powell *et al.* published a direct comparison of the T_{NP} formulae against simulated XPS spectra produced using SESSA, for a range of nanoparticle systems selected to evaluate the T_{NP} method for practically relevant examples. Material systems were chosen so that ratios of effective attenuation lengths of electrons within each material are near to the extremes of what might be observed in reality. Specifically, this covered Au/C, C/Au, Al/Cu and Cu/Al core/coating systems, with core diameters in a range from 1 nm to 200 nm, and coating thicknesses from 0,25 nm to 3 nm. Figure 4 and Figure 5 show the ratio of the thickness calculated using the T_{NP} method to those used for the simulation for the Al/Cu and Cu/Al nanoparticle systems, i.e. those in which elastic scattering is likely to be significant factor. It can be observed from these that, as long as EAL's are used in the calculations, the deviation between these two methods is typically less than ~10 %.

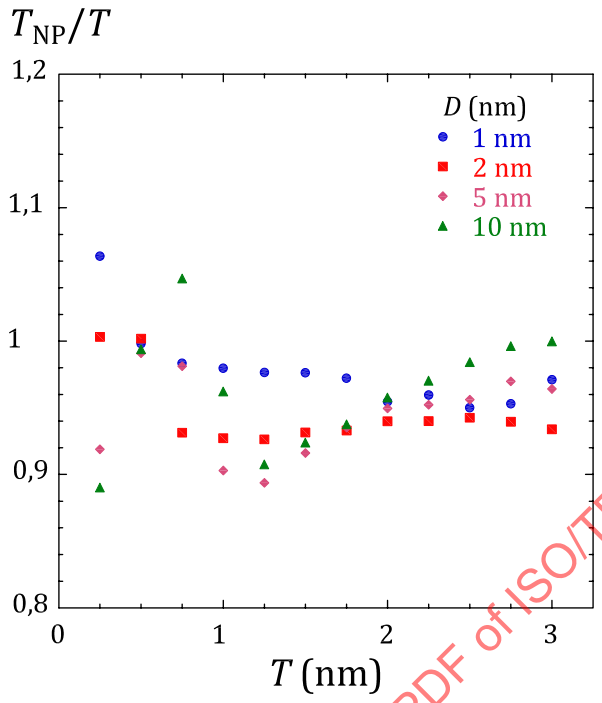

a) For 1 nm to 10 nm core diameters

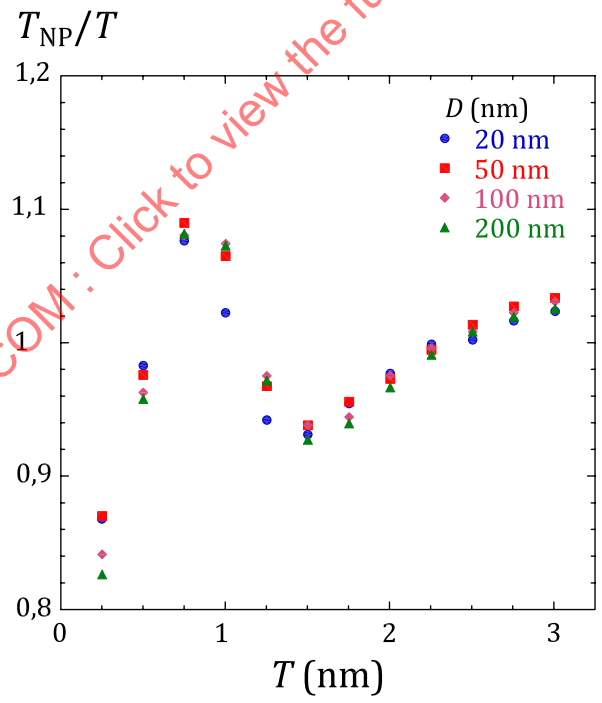

b) For 20 nm to 200 nm core diameters

Figure 4 — Ratio of T_{NP} to SESSA simulated shell thickness (T) plotted as a function of shell thickness (T) calculated from simulated spectra for Cu-core, Al-coated nanoparticles for 1 nm to 200 nm core diameters (D)

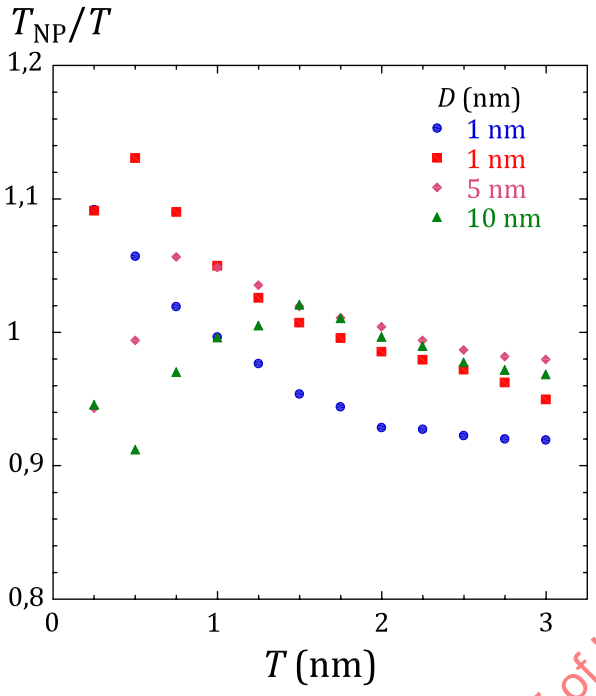

a) For 1 nm to 10 nm core diameters

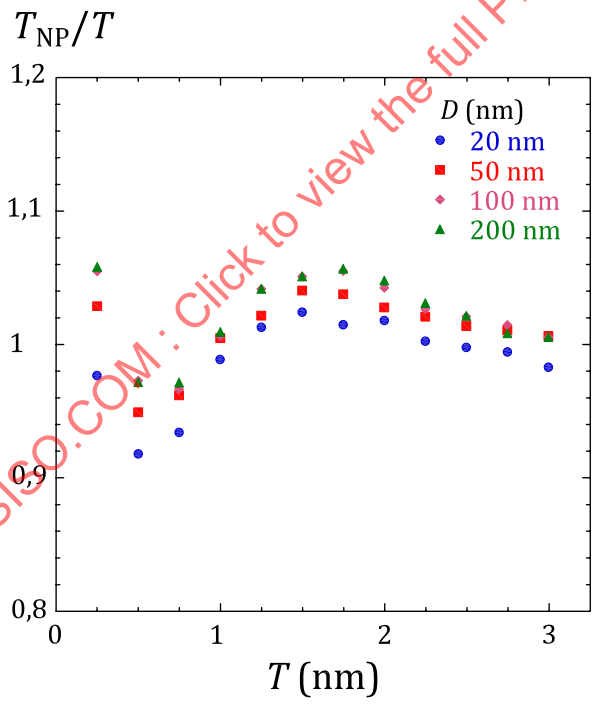

b) For 20 nm to 200 nm core diameters

Figure 5 — Ratio of T_{NP} to SESSA simulated shell thickness (T) plotted as a function of shell thickness (T) calculated from simulated spectra for Al-core, Cu- coated nanoparticles for 1 nm to 200 nm core diameters (D)

Comparisons between different descriptive formulae have also been reported. Figure 6 shows a comparison between results from the T_{NP} method and the method of Gillet and Meunier[28], performed for synchrotron XPS data at a range of photon energies from nanoparticles with a noble metal core, and an Fe_2O_3 shell. Good agreement between these two methods is observed in most cases except for a single datapoint obtained at 200 eV kinetic energy for the Rh-core Fe_2O_3-shell particles[41].

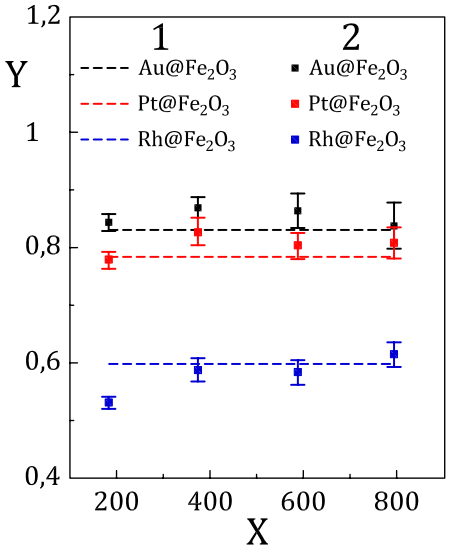

Key

X kinetic energy (eV)

Y shell thickness (nm)

1 Gillet and Meunier

2 T_{NP}

NOTE The same core radius and the experimental integrated intensity ratios were used in each model[41].

Figure 6 — Comparison of shell thickness obtained by Gillet and Meunier's method (dashed lines) and the T_{NP} (square points) equation for particles with noble metal cores and Fe_2O_3 shells

6.8 Inelastic background analysis

Analysis of the background signal in XPS, formed predominantly of photoelectrons that have undergone inelastic scattering before detection, is not commonly applied in the current literature. In many practical analyses, the inelastic background is considered only with respect to how it can most accurately be removed in order to facilitate quantification of a photoemission peak. Despite this, much effort has been put into describing the form of the inelastic background, and how additional information regarding a sample might be extracted from it[42]–[47].

Simple visual inspection of the inelastic background shape can provide useful qualitative information regarding the structure of a given sample, particularly with regards to the presence of an overlayer. Typically, the background immediately below a peak in kinetic energy will show a sharp rise followed by a steady approximately-exponential decay; for a material that is located beneath an overlayer of a different material, there will be a more gradual rise in the background intensity, with a maximum intensity further from the position of the peak. Similarly, an overlayer material will retain the sharp increase in background intensity immediately below the peak in kinetic energy, however the decay in background intensity will itself be sharper.

Careful quantitative analysis of the inelastic background can provide information from a much greater depth within a sample than is typically expected from XPS, approximately 3 times the depth of that available by peak analysis[47]. Where available, background analysis is best performed using software which is capable of providing an accurate simulation of the XPS spectrum, such as QUASES[48]–[51] or SESSA[33],[52],[53]. If such software packages are not available, reasonably practical models have been demonstrated for direct application by the user[47],[54].

Modelling of the inelastic background has not yet been optimised for application to nanomaterials, however such methods can reasonably be applied with some care and forethought. As with several of the peak-based overlayer thickness methods discussed earlier in 6.4, and 6.5, most background analysis

does not directly model elastic scattering and is therefore best used where elastic scattering is not significant (e.g. for organic overlayers) – tools such as SESSA, which attempt to comprehensively model electron trajectories, including elastic scattering, are the exception to this. Another issue can arise from the distinction between the core of a nanoparticle and the effectively semi-infinite substrate considered for planar samples; contributions to the background will arise from beneath the outermost layer of nanoparticles. This is particularly likely to be an issue for nanoparticles with a core radius on the order of 20 nm or smaller. Another issue arises from the 'side' portions of the nanoparticle coating – unlike with planar systems, as the coating thickness is increased, so is the ratio of the cross-sectional areas of the coating to the core, as viewed from the detector. This method is therefore most valid for particles in which the ratio of core radius to coating thickness is large. SESSA simulation of the Cu 2p spectra for Au/Cu, Cu/Au, and Au/Cu/Au nanoparticle systems performed by Powell *et al.* demonstrated the difference in the inelastic background for nanoparticle core and overlayer materials across a range of different dimensions. These spectra demonstrate how qualitative inspection of the inelastic background above a peak can be used to infer nanoparticle morphology[55], an example of this for the Cu/Au particles is shown in Figure 7; the intensities shown are normalised to the peak height, thus illustrating only the change in the relative intensity of the background and the peak with changing overlayer thickness. An increase in the overlayer thickness results in a corresponding increase in the background relative to the peak itself. When comparing the models with elastic scattering to those without, it can be seen that the effect of elastic scattering is to slightly reduce the intensity of the background relative to the peak, as elastically scattered electrons will contribute to the peak signal. In reality, this corresponds to the differences observed between overlayers of low-Z elements (weak elastic scattering) compared to high-Z (strong elastic scattering).

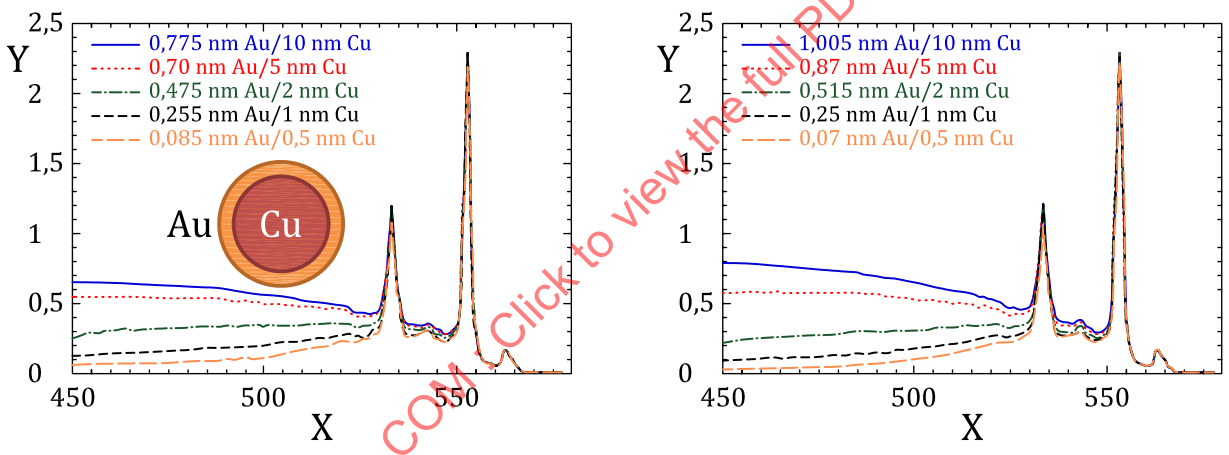

a) With elastic scattering **b) Without elastic scattering**

Key

X electron energy (eV)

Y relative intensity

Figure 7 — Spectra simulated for the Cu 2p peak region from Cu-core, Au-shell nanoparticles with a range of core diameters, and shell thicknesses set such that the peak intensities match to within 2 %[55]

6.9 Elemental composition

For standard XPS measurements of composition, it is assumed that within the observed sampling depth of the technique, the sample material is of a uniform, homogeneous composition. Atomic concentrations calculated from peak intensities are typically given based on this assumption. In the case of a substrate/overlayer system, potentially determined by observation of the inelastic background as described above, this assumption is invalid. Differential attenuation of electrons with differing kinetic energy through an overlayer will result in measured peak intensities that are not in proportion to the composition of the substrate; likewise, the finite thickness of the overlayer will skew the measured composition, although

this effect is less significant, and reduces as the overlayer thickness tends towards the maximum information depth of a given x-ray source. Figure 8 shows a schematic illustration of this concept.

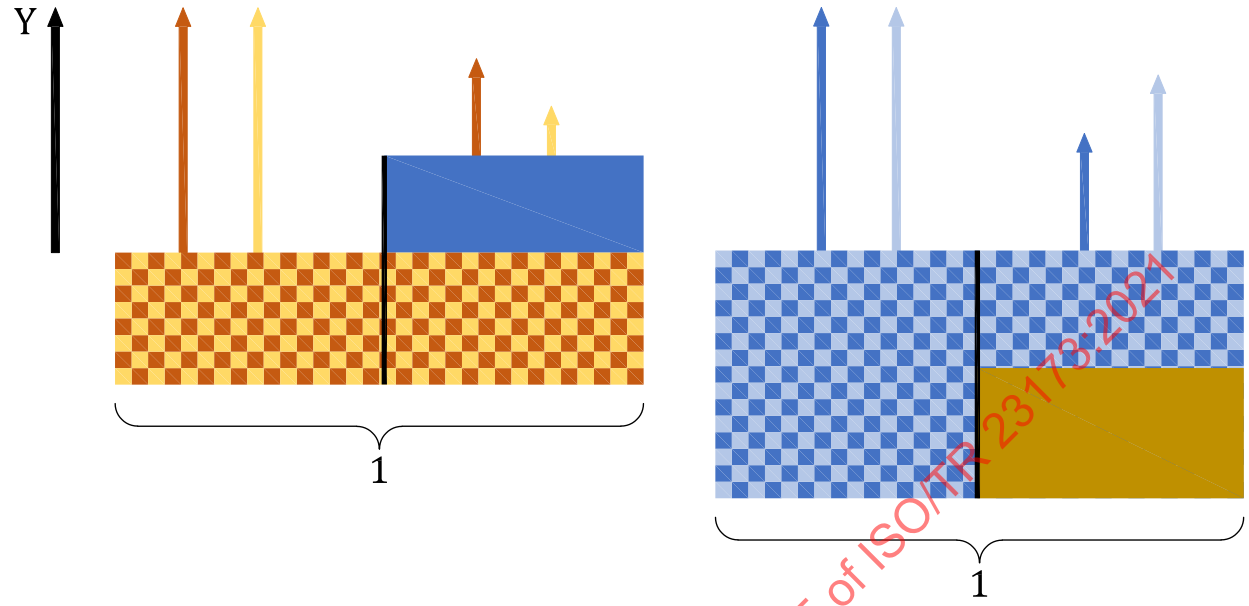

a) b)

Key

Y	arrows represent sensitivity adjusted XPS signal
1	sample depth beyond base of schematic significantly greater than effective attenuation lengths
	higher kinetic energy electrons
	lower kinetic energy electrons

NOTE Each arrow represents the signal intensity, corrected for the appropriate pure-material intensity, i.e. $I_x/I_{x,X}$. Substrate materials are considered to extend to a depth much greater than the relevant EAL. Darker shaded arrows represent signal from higher kinetic-energy electrons. For a substrate material (a), the concentration of elements from higher kinetic-energy peaks will be overestimated relative to the pure composition, whereas for an overlayer (b), the concentration from higher kinetic energy peaks will be underestimated.

Figure 8 — Schematic illustration of the effects of a layered structure on the measured concentration of elements within the substrate and overlayer

For most systems, this discrepancy can be corrected for in the process of determining overlayer thickness. To do this, all initial assumptions required for the estimation of the overlayer thickness need to hold true, particularly that the substrate/core and overlayer materials are uniform and homogeneous. Additionally, it is necessary to assume that if estimating effective attenuation lengths, that a mean value calculated using stoichiometrically weighted parameters (e.g. atomic number) is valid. In this case, the analyst can calculate an overlayer thickness using their preferred method for each substrate/overlayer element pair. Effective attenuation lengths can be estimated from formulae[26],[29],[30] using stoichiometrically weighted values (or obtained from a database such as the NIST EAL database[31]), and likewise pure material reference intensities can be adjusted to match the estimated stoichiometry. The array of overlayer thicknesses thus calculated will likely vary between element pairs if the estimated composition is incorrect. By varying the composition in order to obtain a minimum deviation between estimated overlayer thicknesses from different element pairs, a more accurate estimate for the compositions can then be obtained. This iterative method was shown using the T_{NP} equation for a well-characterised system consisting of a known organic coating on gold nanoparticles[27].

This has further been demonstrated for gold nanoparticles coated with a self-assembled monolayer possessing a significant compositional difference between the two ends of the molecule coating the

gold core as illustrated by Figure 9[23]. Both modelling as a single layer, or as a two-layer system using an extension of the T_{NP} method resulted in composition estimates that were reasonably close to that expected for the molecule based on stoichiometry, with slightly greater accuracy when modelled as a two-layered system. This method is equally applicable to inorganic coatings and samples of any morphology, but does not account for any concentration gradients that can be present.

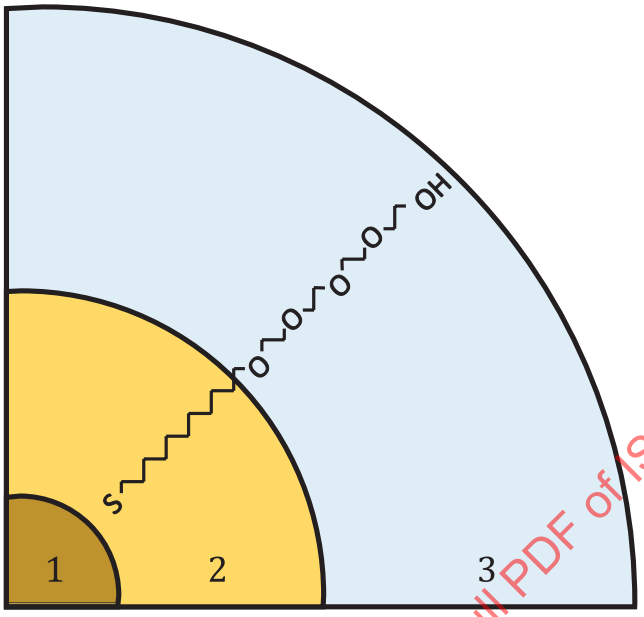

Key

1 core
2 shell 1
3 shell 2

Figure 9 — Schematic of the system from[23], indicating the two distinct layers within the coating molecule

6.10 Variable excitation energy XPS

6.10.1 General

The intrinsic properties of synchrotron radiation provide exciting and important possibilities to investigate the internal heterostructure of NPs with XPS. Since the first synchrotron was built exclusively for external user operation in 1981 in Daresbury (England, United Kingdom), technical advances have increased the brilliance of the available synchrotron radiation produced by modern light sources by several orders of magnitude[56]. At the time of writing this document, there are approximately 50 synchrotron facilities in operation all over the globe and each of them exhibits at least one beamline equipped with an XPS endstation[57].

X-rays from a storage ring differ from X-rays produced by radiation sources installed in standard lab-based XPS spectrometers. While lab-based X-ray sources provide only one or two characteristic energies (typically Al K_α at 1 486,6 eV and Mg K_α at 1 253,6 eV), the radiation from a storage ring consists of a continuous spectrum from 1 eV up to several GeV. It depends on the specific beamline design which section of this spectrum is extracted and, thus, available at the endstation. Within this section the energy is tuneable using a suitable monochromator system. The tuneability of the X-ray excitation energy leads to a tunability of the XPS information depth and, thereby, enables non-destructive depth-profiling of the chemical composition[58]. Furthermore, higher available X-ray energies not only facilitate the excitation of electrons with higher binding energies, but also corresponds to a greater maximum information depth. Opposed to that, smaller available X-ray energies provide higher surface sensitivity than lab-based X-ray sources. However, the variability and often unique nature of individual synchrotron

stations also renders the analysis of data from such sources increasingly complex compared to that of lab-based sources. The effects of polarization of the x-ray beam; nonstandard geometries of the beam, sample, and detector; and typically un-calibrated analysers require careful consideration - ideally during the planning stage of any given experiment - in order to be able to correctly interpret the data obtained.

With a typical brilliance of 10^{20} photons/s/mrad^2/mm^2/0,1 % bandwidth synchrotron light is many orders of magnitude brighter than X-rays produced by radiation sources in standard lab-based XPS spectrometers with a typical photon flux of 10^9 photons/mm^2/s[56],[59]. The larger number of photons results in higher photoelectron counting rates, better signal to noise ratio, the possibility to choose between the selection of a lower pass energy for advanced energy resolution or shorter acquisition times. Short acquisition times can enable time resolved experiments[60]. High counting rates become especially important when measuring at elevated excitation energies where electron photoionization cross-sections become small and electron analyser transmission is reduced[61]. However, this increased photon flux also significantly increases the risk of damaging samples, particularly those containing organic materials.

6.10.2 Qualitative depth-profiling

Energy resolved and non-destructive depth-profiling by synchrotron-XPS works by varying the photon energy and, thus, the kinetic energy of the photoelectrons. The principle is illustrated in Figure 10. This principle is of special importance when it comes to the analysis of nanoparticles, since angle resolved depth-profiling is not applicable to nanoscale objects with spherical shape.

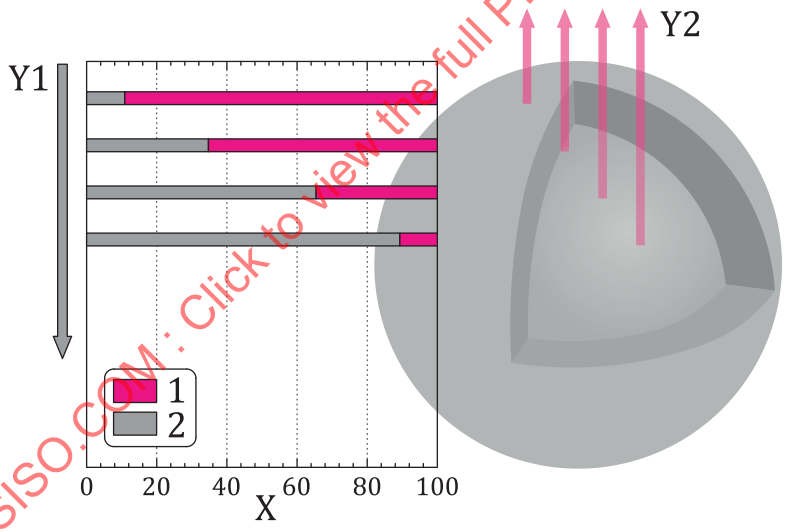

Key

X XPS intensity ratio I(core)/I(shell)
Y1 increasing kinetic energy
Y2 information depth
1 shell material
2 core material

NOTE The increase of the core contribution with increasing kinetic energy is expected when the NP radius is larger than the largest investigated XPS information depth.

Figure 10 — Schematic representation of the XPS intensity ratio of core and shell material in a core-shell NP from the kinetic energy of the photoelectrons or the XPS information depth

If the NP radius is larger than the maximum XPS information depth, it is possible to gain information on the distribution of the different components within the NP core and coating by collecting spectra at two or more photon energies. Here, the superior surface sensitivity of synchrotron radiation is decisive,

since it facilitates information depths small enough to exclusively analyse the surface region of a NP. The photon energy dependence of the XPS intensity ratio of two constituents need to be examined. An independence of the ratio from the photon energy indicates a homogeneous distribution. An increase or decrease of the intensity ratio with photon energy signifies a surface enrichment of one component and an enrichment of the other component in the core, respectively. This is a rather qualitative approach of analysing the internal structure of NPs.

It is advisable to select different photon energies for different components, such that their kinetic energy is similar within the range of a few eVs, in order to enhance the accuracy of the measurements[62]. In this case, the XPS intensities are normalized only by the respective photoionization cross-sections to become comparable. However, if the kinetic energies are significantly different, XPS intensities need to be additionally normalized for the effective attenuation length[63] of the photoelectrons as well as the electron analyser transmission function[58]. These corrections are of course not required if different species within the same core-level spectrum are compared (e.g. Si2p photoelectrons from Si^0 and Si2p photoelectrons from Si^{4+}).

Feng Tao *et al.*[64] demonstrated such a qualitative approach for unsupported $Pt_{0,5}Pd_{0,5}$ model NP catalysts with an average radius of 7,5 nm, measured at selected photon energies corresponding to IMFPs from 0,7 nm to 2 nm. The XPS intensity ratios of Pt4f and Pd3d yielded a relative atomic fraction ranging from 84 % ± 3 % Pd for the lowest IMFP, to 52 % ± 3 % Pd for the highest (see Figure 11). Based on this depth profile the authors concluded a core-shell particle structure with a Pd enriched shell and a Pt enriched core. A very similar system of $Pt_{0,7}Pd_{0,3}$ was analysed via synchrotron-XPS in a more quantitative manner by Bernardi, et al.[65]

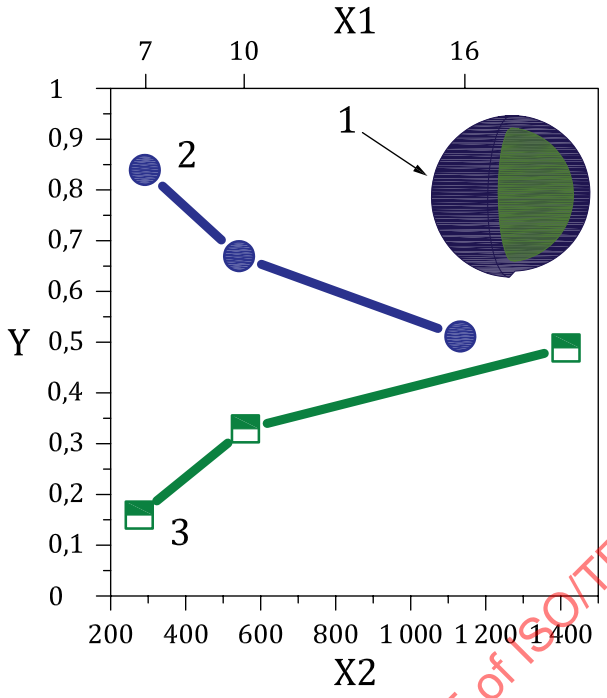

Key

X1 inelastic mean free path (Å)
X2 kinetic energy (eV)
Y atomic fraction
1 pd-rich shell
2 palladium
3 platinum

NOTE Schematics showing the core-shell structures of the $Pt_{0,5}Pd_{0,5}$ NP is included (this schematic does not represent the shape of the NP). The y-axis data points have an associated error of ±0,03[64].

Figure 11 — Dependence of Pd and Pt atomic fractions of the as-synthesized $Pt_{0,5}Pd_{0,5}$ measured in ultra-high vacuum (UHV) at 25 °C as a function of the kinetic energy (KE) and inelastic mean free path of the excited photoelectrons

The quantitative interpretation of the dependence of the relative XPS intensities on the photon energy can also be applied to characterize the interface between NPs and the shell composed of the organic stabilizer or capping agent. Information about this interaction is hard to obtain with any other analytical technique and particularly crucial in the field of semiconductor quantum dots, in order to explain the photoluminescence properties[41],[66],[67]. These methods of qualitative depth profiling and chemical analysis using variable-photon-energy XPS have been demonstrated for a number of different systems, several examples of this type of analysis are summarized in Table 2.

Table 2 — Examples of the application of synchrotron XPS to a range of different nanoparticle systems.

Core	Shell	Diameter (nm)	Photon energy range (eV)	Notes	Reference
$NaYF_4$	$NaGdF_4$	21	250 - 1 050	Analysis confirmed the likely core-shell nature of the particles from the observed changes in Y:Gd ratio with changing photon energy	[68]
InP	ZnS	3,6; 5,1	546 - 986	Structural differences arising from synthesis routes were identified	[69]
Sb_2O_5-SnO_2	IrO_2-RuO_2	29	100 - 1 400	Two possible morphologies were identified that could give the observed results	[1]
LaF_3	GdF_3/LaF_3	3-10	900 - 1 200	The nanoparticles were shown to have a 'core-shell-shell' morphology with La concentrated in the core and outer shell, with a Gd layer between.	[70]
CdS	MPA (mercapto-propanoic acid, an organic capping agent)	2,7 - 7	203 - 500	The chemical species present at the core-shell interface were identified for the S 2p signal, and variation in interfacial chemistry with nanoparticle size was identified	[71]
InAs	TOP (trioctylphos-phine, an organic capping agent)	3,7 - 6	89 - 578	Separate surface and core species were identified for both In and As peaks – this allowed characterisation of relative surface: volume ratios for the different sizes of particle	[72]

6.10.3 Quantitative depth-profiling

By simulations of theoretical XPS intensities assuming a suitable model morphology, it is possible to model the dimensions of the NP (shell thickness, core and total diameter). The possibility to extract the thickness of NP coatings from XPS intensities is of interest when investigation with TEM comes to its limits. This is the case as soon as the core and shell materials exhibit insufficient image contrast; if the core and shell material have similar lattice constants; if the shell is very thin; and in situations with defects and disorders connected with the core-shell interface region[73],[74]. Note that the coating thickness can be calculated by lab-based XPS from only a single pair of XPS intensities of core and shell materials as described previously. However, the advantage of synchrotron-XPS is that by the recording of several pairs of XPS intensities at varying information depths more information can potentially be obtained, thus providing greater insight or a more accurate result[75]. Several examples of the application of quantitative depth-profiling by means of synchrotron-XPS are summarised in Table 3.

Table 3 — Examples of the application of quantitative synchrotron XPS analysis to a range of different nanoparticle systems.

Core	Shell	Diameter (nm)	Photon energy range (eV)	Notes	Reference
InP	ZnS/TOP (Organic capping agent)	8	540 - 1 300	Simulated data based on a core-shell-shell structure with a constrained core radius was fit to the experimental data, providing estimates for both the ZnS and organic capping thicknesses.	[76], [74]–[79]
Au; Pt; Rh	Fe_2O_3	5	250 - 1 500	Increasing core:shell intensity ratios with photon energy confirmed the noble-metal-based core. A simple ideal core-shell model was used to estimate shell thickness, however for the Rh-core particles this could only be fit to the experimental data at all photon energies with the inclusion of Rh in the shell. This demonstrates a circumstance where analysis at multiple photon energies can provide additional information. Comparisons between descriptive formulae[24],[28] were also performed, and showed good agreement at all photon energies.	[41]
PbSe	TOP (Organic capping agent)	3; 9; 11	200 - 800	Used simulation to quantify the PbSe species present at the interface between the particle and the organic capping ligand. The obtained results were used to explain the different photoluminescence properties of the various particle sizes.	[80]
ZnS	CdSe-ZnS	3,7	615 - 1 486	The interfacial regions of ZnS-CdSe-ZnS nanoparticles were investigated using synchrotron XPS. Simulations, constrained by information from complementary techniques such as TEM and inductively coupled plasma atomic emission spectroscopy (ICP-AES), were used to establish the structure of the particles. The structure found to be consistent with all experimental data was that of a gradient interface between the ZnS core and CdSe first shell, and a sharp interface between the CdSe first shell, and the ZnS outer shell.	[73]

6.11 Near-ambient-pressure XPS (NAP-XPS)

6.11.1 General

Due to the strong scattering of electrons by matter, XPS experiments are usually conducted in UHV conditions. However, such conditions can lead to significant limitations when it comes to the characterization of NP coatings. Many NPs are synthesized in liquid suspension and need to be transferred to a dry state for experiments in UHV. The influence of the drying and evacuation processes on the particles' chemical and physical properties is hard to estimate. Therefore, it is of high interest to acquire spectra in the same gaseous or liquid environment which is used for the synthesis or the application of a given nanoparticle system, to ensure the relevance of the information provided by XPS. Modern NAP-XPS instruments are usually composed of a sample chamber at elevated pressure which is connected to the electron analyser and detector via a differentially pumped electrostatic lens system[81]. NAP-XPS in combination with synchrotron radiation is an frequently used approach where the high brilliance and small beam size are exploited[82]. So far, the investigation of nanoparticle coatings has almost exclusively been performed at synchrotrons, however there is a growing number of studies performed on lab-based instruments.

6.11.2 Internal structure of bimetallic NP catalysts

NPs are of interest in the field of heterogeneous catalysis, because their enhanced surface-to-volume ratio can substantially increase the efficiency of a catalytic process[83]. Quite often NPs comprising two metal components exhibit higher catalytical activity, selectivity and stability than their monometallic counterparts[84]–[86]. The catalytic reaction takes place at the NP/atmosphere interface. To understand the mechanism behind and, thus, to optimize the catalyst performance, it is crucial to know how the surface chemical composition changes with the surrounding conditions. NAP-XPS facilitates monitoring of this surface composition as a function of nature and pressure of the surrounding gas atmosphere as well as of temperature. Table 4 summarises several examples of the application of NAP-XPS for such systems, also including some obtained using lab-based systems.

Table 4 — Examples of the application of NAP-XPS for characterising the nature of catalytic nanoparticle surfaces

Core	Shell	Diameter (nm)	NAP conditions	Notes	Reference
Rh, Pd	Pd, Pt,	8 - 16	0,13 mbar; NO, O_2, H_2, CO; 573 K	RhPd and RhPt systems exhibited different surface chemistry dependent on the gas present, while PdPt was unchanged	[86], [64], [87]–[89]
Rh	Pd	4	0,05 mbar; O_2, H_2, C_2H_5OH; 573 K, 823 K	Particles were investigated unsupported and on CeO_2 supports, and showed reduced activity on supports, indicating the importance of 'realistic' test conditions	[90], [41], [91]
Pt	Co	3	0,2 mbar; O_2, H_2; 520 K	Demonstrated that a desired behaviour (reduction of oxides) under specific conditions was present in a nanoparticle sample but not in the bulk	[92], [84], [91], [93]
Cu	Co	22	1,3 mbar O_2; 6,7 mbar H_2; 523 K, 603 K	Demonstrated morphological and compositional changes occurring under redox cycling	[94], [95]
Pt; Pd	Pt	3; 12	Lab-based system; Various pressures of CO between $2,7 \times 10^{-10}$ and 6,7 mbar, 293 K	Identified formation of undercoordinated Pt atoms on the surface at pressures above 0,2 mbar for both pure Pt and Pd/Pt particles	[96]
Au	Ni	15-28	Lab-based system; O_2 at 10^{-1} and 10^{-3} mbar, 323/373 K	Identified Ni oxide formation on all shells except the thinnest, consistent with enhanced catalytic activity of the thinnest-shell particles.	[85]
Cu	Ni	15	Lab-based system; oxygen-plasma-treated before analysis, then 1 mbar H_2 at 523 K in NAP system	Core-shell structure presumed to form during oxidation and is preserved during reduction. Improved catalytic activity and selectivity noted after treatment	[97]

6.11.3 Measurement of NP's in liquid suspension

One significant advantage of NAP-XPS is the possibility of investigating nanoparticles in liquid suspension, and thereby directly measuring the liquid/nanoparticle interface. Currently the most popular technical solution for this is the liquid microjet method. The basic principle of such an experiment is explained here using the set-up at the Swiss Light Source as an example (see Figure 12, right). The nanoparticle suspension enters the analysis chamber through a nozzle of diameter 28 to 50 µm with a flow rate of approximately 75 ml/min, travels a distance of 1,5 cm through the chamber and then exits through a 600 µm hole in an aluminium catcher (see Figure 12, left). X-rays hit the liquid jet and photoelectrons are collected and guided toward the energy analyser through a differential pumped electron optical system. Measurements can be performed at pressures in the analysis chamber between 10^{-3} and 20 mbar, while for a detailed XPS experiment where several survey and high-resolution spectra

are acquired 100-200 mL of suspension is necessary[98],[99]. The quantitative evaluation of XPS depth-profiles for shell thickness determination of NPs in liquid suspension is currently still difficult; this is mainly due to a lack of data regarding the IMFP of the photoelectrons in the solvent and the complex spatial distribution of NPs at the liquid/atmosphere interface[100]. Table 5 summarises examples for the application of NAP-XPS for NPs in liquids.

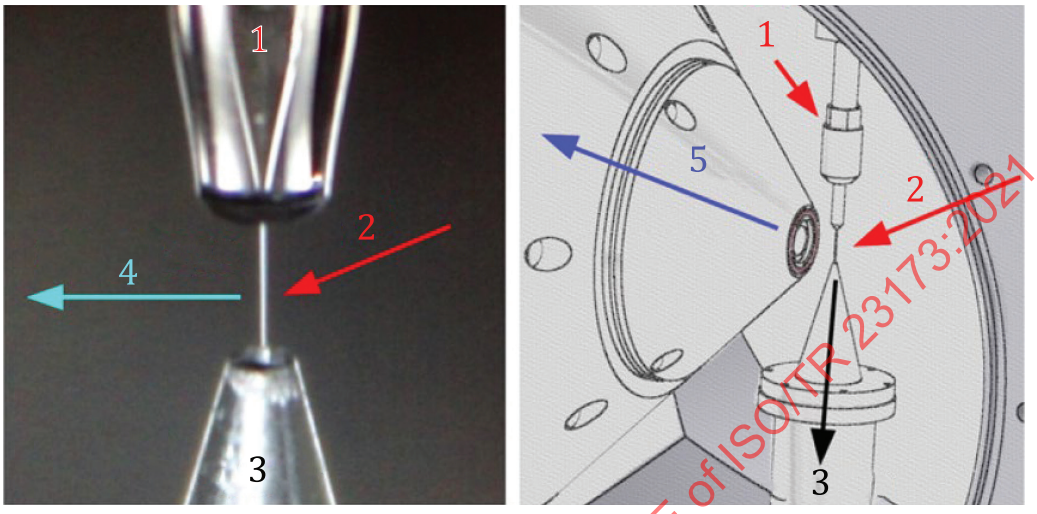

a) Schematic showing positions of jet, photons, catcher and electrons

b) Schematic showing that the incident photons, and the axis of the electron optical system (leading towards the detector) are all normal to one another

Key

1 jet
2 photons
3 catcher
4 electrons
5 detector

NOTE 1 The direction of liquid flow is from top to bottom. The liquid is expanded at a velocity of ~50 m/s into the measurement chamber through a micron sized quartz nozzle. Measurements can be performed at pressures in the analysis chamber between 10^{-3} and 20 mbar. The liquid filament is then irradiated with X-rays before being "caught" by the catcher and removed from the measurement chamber.

NOTE 2 See Reference [99].

Figure 12 — Schematics of a 50 µm liquid microjet in operation at the Swiss Light Source

Table 5 — Examples of the application of NAP-XPS for analysis of nanoparticles in liquid

Core	Shell	Diameter (nm)	NAP conditions	Notes	Reference
SiO_2	Organic	70	Deionised water liquid jet; nanoparticle concentration of 9×10^{12} ml^{-1}	Observed a change in chemical species observed for Si between UHV and in liquid – proof of principle that such information can be obtained	[101]
SiO_2	$Si\text{-}O^-$	7	20 w% aqueous suspension of nanoparticles in liquid jet	Multiple photon energies were used, and an estimate for the thickness of the shell formed by interaction with the water was obtained, after careful consideration of the attenuation of the electrons through the water itself	[102]
SiO_2	Al_xO_y	12	10 w% aqueous suspension of nanoparticles in liquid jet	No quantitative estimate of shell thickness was considered possible as yet, but the core-shell structure of the particles was confirmed by observing core/shell peak intensities as a function of photon energy	[100], [103]
Ag; CaF_2/SrF_2	Ag; SrF_2/CaF_2	20; 5-10	Ag in aqueous solution; CaF_2/SrF_2 and SrF_2/CaF_2 in ethylene glycol	Demonstration of lab-based analysis of nanoparticles in suspension without the use of the liquid jet method or any solution replenishment – direct introduction of solution to the instrument. Identified a chemical difference between wet and dry Ag particles, while no change between dry and suspended CaF_2/SrF_2 or SrF_2/CaF_2 was observed.	[104]

7 Auger electron spectroscopy

7.1 General

AES is based on the Auger effect, in which incident radiation leads to the ejection of a core level electron, and the generated core hole is filled by an electron from a higher energy level. This results in the emission of an Auger electron with a defined kinetic energy dependent on the energy difference between these three energy levels[105].

Like XPS, the information depth in AES is not determined by the penetration of the material by the incident radiation, but by the IMFP of the Auger electrons leaving the sample. Consequently, AES is a surface-sensitive technique with an analysis depth usually between 0,4 nm and 5,0 nm[32],[106].

AES instruments can be operated in spectroscopy or imaging mode. In the following, the advantages and also difficulties of the different operation modes for NP characterization will be discussed. This document is focused on electron excited Auger experiments, as opposed to X-ray excited Auger experiments. Modern electron guns facilitate measurements with small incident beam diameters and, thus, high lateral resolution below 10 nm, which is useful for the investigation of nanoscale objects.

7.2 Coating thickness measurement

7.2.1 General

There are several ways to determine nanoparticle coating thickness by AES. Which one is applied depends on the dimensions of the nanoparticle and its coating relative to the AES information depth. As soon as the coating thickness exceeds the AES information depth, destructive depth-profiling

techniques can be applied. However, if the coating thickness is lower than the AES information depth non-destructive depth-profiling is possible by exploiting the dependence of the IMFP of the Auger electrons in a material on their kinetic energy. Several examples of the methods described here are summarised in Table 6 at the end of this clause.

7.2.2 Destructive depth-profiling

Destructive depth-profiling can be performed by gradually removing material through sputtering with, for example, an Ar^+ ion beam. Quantitative spectral analysis at different points throughout the sputtering yields a depth-profile of the chemical composition of the sample. Another form of destructive-profiling which can be applied to coated nanoparticle samples is cross-sectioning (for instance by freeze fracturing, microtomy, focused ion beam or ion milling) and subsequent AES elemental mapping or line scan analysis of the cross-cut nanoparticles. Destructive techniques are only preferred over non-destructive ones when chemical information is required from a depth that exceeds the intrinsic information depth of the AES measurement. As it is often hard to estimate the effects that sputtering or cross-section sample preparation have on the NP chemical composition and morphology. Sputter depth-profiling in particular is a complex process and various factors need to be taken into account, mainly including preferential sputtering as well as sputter-induced roughness, mixing effects and chemical reactions[105]. A further problem specifically related to NP characterization is a higher sputter yield of NPs compared to the corresponding bulk materials which is related to the larger surface area of the particles and the smaller volume for dissipation of the primary ion energy. The same reasons can also cause melting of the particles under primary ion beam irradiation[107].

7.2.3 Non-destructive depth-profiling

Non-destructive depth-profiling by AES can be achieved by exploiting the dependence of the IMFP, and thus the information depth in a material, on the kinetic energy of the Auger electrons. The simplest estimation of a NP shell thickness is to calculate the information depth of the lowest kinetic energy peak of the core material that is visible in the spectrum. This yields an upper limit for the shell thickness, certainly based on the assumption that encapsulation of the core by the shell material is complete. Likewise, a lower limit for the shell thickness is given by the information depth peaks from the core material that are not observed in the spectrum. Furthermore, it is possible to estimate a NP shell thickness by comparison of the peak intensities of two Auger transitions from the same element (e.g. KLL and LMM) of different kinetic energy and, thus, different IMFPs. Well established formulae for overlayer thickness estimation on planar samples cannot be applied to NPs due to their topography. Instead suitable simulation software such as SESSA[22],[108] with corresponding model morphologies can be used. The T_{NP} formula or numerical models described for XPS can also be applied to AES data, however under the additional required assumption that excitation is uniform across the analysed depth.

7.2.4 Elemental composition

As well as Auger peaks, after electron impact AES spectra additionally contain a background generated by inelastically scattered electrons and further secondary electrons. As Auger signals are very small in comparison to this background, normally the differential representation of the spectrum is used[105]. The operator of a modern Auger electron spectrometer has two options for spectral characterization of nanoparticles. Either a spectrum with the high spatial resolution is recorded to identify the chemical composition of a single nanoparticle or a small nanoparticle aggregate (spectral point analysis mode), or a spectrum at low spatial resolution is recorded to identify the average chemical composition of a large NP ensemble (spectral ensemble analysis mode). While both methods are useful, spectral point analysis can be considered the most important, as ensemble analysis can be performed with most electron spectroscopies, whereas analysis of a single nanoparticle is a capability limited to the use of electron-gun-based AES.

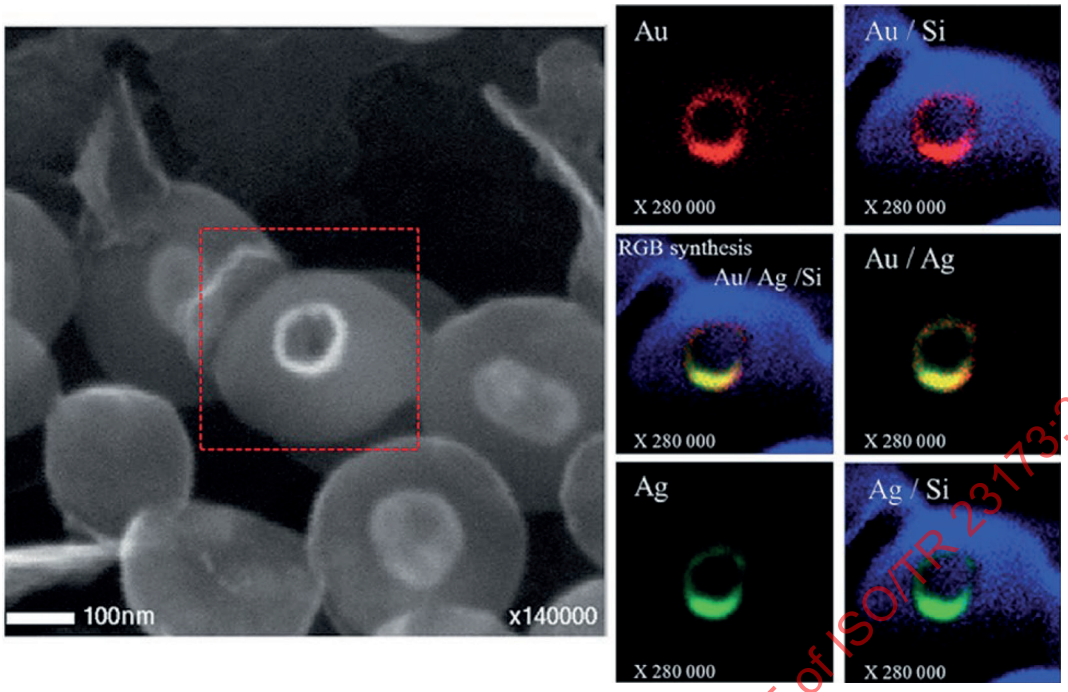

a) SEM image of cross-cut AgAu-core, SiO_2-shell NPs

b) Element scanning Auger microscopy (SAM) overlays

NOTE 1 The red dotted line indicates the specific CSNP that is investigated by AES elemental mapping.

NOTE 2 Red [Au(MNN)]; green [Ag(MNN)]; blue [Si(KLL)]

NOTE 3 See Reference [109].

Figure 13 — Example of ion-milling and elemental mapping for nanoparticle analysis

7.2.5 Imaging and line scans

The high spatial resolution of AES facilitates the generation of elemental maps and lines scans on the nanoscale. It is even possible to investigate single NPs. It is worth noting that the spatial resolution of AES is always worse than the beam diameter of the incident electrons. The cause of this is the backscattered electrons that excite Auger electrons within a certain volume outside the primary beam irradiated area. Additionally, in the case of NPs distributed on a substrate, the so-called edge effect can lead to a decrease in spatial resolution. The edge effect corresponds to primary electrons that are scattered within the NP and, thus, hit the surrounding substrate which leads to Auger excitation[110]. A combination of both phenomena leads to the substrate signal being detected even if the NP diameter exceeds the primary beam diameter and the beam is focused on the NP centre. This is illustrated in Figure 14 where two Au-Ag core-shell NPs of 20 nm and 60 nm diameter are investigated by AES line scan analysis. In both cases, the Si(KLL) signal from the substrate decreases when scanning across the NPs to about 50 % compared with the intensity outside the NP.

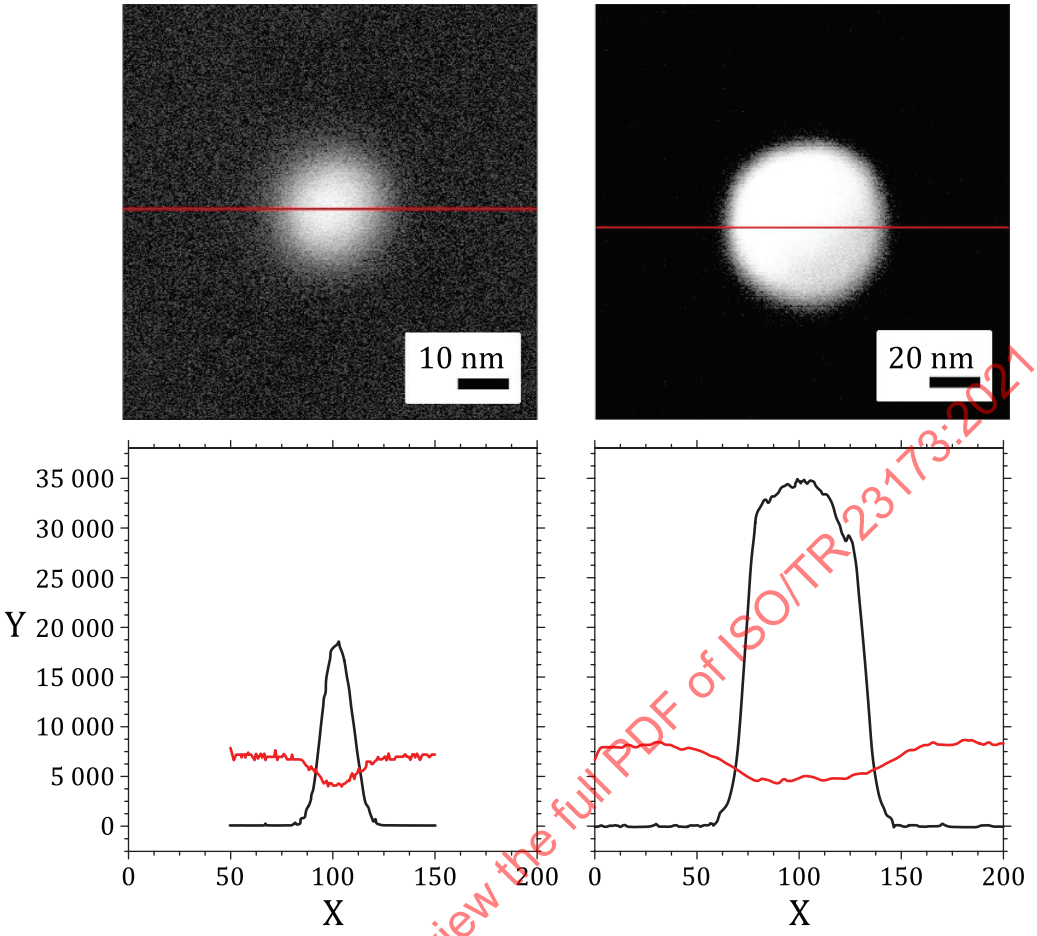

Key

X position (nm)

Y intensity (arb. units)

NOTE Auger electron spectroscopic linescans (lower panel) of the elements silver and silicon of an Au-Ag core-shell NP with 20 nm total diameter (left) and 60 nm total diameter (right). Electron micrographs with red lines indicates the position of each corresponding linescan (upper panel).

Figure 14 — Auger electron spectroscopic linescans and electron micrographs of Au-Ag core-shell nanoparticles

The extent of the edge effect depends on the kinetic energy of the incident electron beam which was demonstrated by Ito, et al.[110] who performed AES line scan analyses of 300 nm Al_2O_3 particles. It can be shown that for a line scan performed at 20 kV the number of forward scattered electrons is reduced by a factor of two compared with a line scan at 5 kV. Consequently, the edge effect is reduced and the spatial resolution enhanced for NP characterization with high primary electron kinetic energy[110]. The issue of artefacts related to edge and backscattering effects has been further addressed using Monte Carlo simulations by Li, et al.[111] It is concluded that the quantitative evaluation of AES images and line scans is only valid after careful consideration of the possible influence that contrast artefacts could have had on the measurements.

Table 6 — Examples of the application of AES depth-profiling, compositional analysis, and imaging

Core	Shell	Diameter (nm)	Analysis applied	Notes	Reference
SiO_2	Fe_3O_4/Organic	250 (SiO_2); 10 (Fe_3O_4)	Destructive: Ion sputtering	Investigated silica microspheres coated with multilayered structure formed of Fe_3O_4 nanoparticles and a polyelectrolyte. Destructive depth profiling was used to characterize the layered structure.	[112]
AuAg	SiO_2	280	Destructive: Ion milling cross-section Elemental mapping	Hollow-core-shell structure of the nanoparticles was visualized using a combination of ion-milling and SAM elemental mapping (see Figure 13). Line-scan analysis revealed a heterogeneous distribution of Au and Ag within the core.	[109]
SiO_2	C	~20	Non-destructive: Auger peak comparison	Coated and uncoated particles were compared; by using a comparison between high KE (IMFP ~12 nm) and low KE (IMFP ~2,2 nm) auger transitions, coating thickness was estimated	[113]
CuO	LiO_2	<50	Elemental composition by spectral point analysis	Spectral point analysis of CuO nanoparticles during in-situ Li-ion cycling revealed the formation of LiO_2 at the nanoparticle surface, and that this could be partially reversed.	[114]
ZrO_2	Al_2O_3	~62 (5 – 200)	Elemental mapping	Imaging of Zr(LMM) and Al(KLL) used to demonstrate that Al_2O_3 formed a coating across the entire surface of the nanoparticles	[115]
Ag	Antibody functionalised	Aggregates <100 nm	Elemental mapping	Attachment of Ag nanoparticles to a U937 leukaemia cell were demonstrated by the use of elemental mapping of C(KLL), O(KLL), and Ag(MNN) Auger peaks.	[116]
Cu; SiO_2; SiC	-	-	Elemental mapping	Elemental mapping of SiO_2 nanowires was able to identify the Cu seed particle at the base of the wire. Line-scans of SiC nanodots demonstrate agreement with electron microscopy.	[117]
SiO_2	C (contaminant)	30 nm	Elemental mapping; Line scans	AES mapping and line scans of single SiO_2 nanoparticles were performed, showing the effects of a carbon contamination layer and various artefacts that occur at the edge of nanoparticles for AES line scans.	[118], [119]

8 Complementary analysis

When interpreting electron spectroscopy data from coated nanoparticles, and particularly when attempting quantification of coating thickness, many of the methods discussed require a significant number of assumptions regarding the nanoparticle system itself. Likewise, certain pieces of information, such as size, are likely required for some methods before an estimate of coating thickness can be made. Many assumptions can be ratified using complementary analytical techniques; likewise, any information required for a calculation of coating thickness that cannot be obtained using electron spectroscopy, can be obtained using another technique. Care shall be taken, however, to ensure the

relevance and correct interpretation of data from other techniques when utilised for analysis of electron spectroscopy data. A common example is the difference between measurements of size made using many solution-based techniques, compared to those made in dry or vacuum conditions; the relevant 'size' of a particle for techniques which rely on motion within solution is the Stoke's diameter, which is distinct from the actual physical diameter of the particle. Related to this is the potential for changes to occur in terms of size and morphology of particles in solution as compared to when dry, due to potential hydration of the surface, or changes in surface energy in different environments.

Table 7, below, lists many commonly used techniques for the analysis of nanoparticles, alongside the benefit they provide in complement to electron spectroscopy measurements, and any associated disadvantages.

Table 7 — Complementary analysis techniques, with their benefits and disadvantages for assisting in electron spectroscopy measurements of coating thickness

Technique	Benefits	Disadvantages
Size determination		
Size is required for any overlayer thickness calculation from electron spectroscopy data		
SEM and TEM	Can provide information on size and shape of particles to support/refute assumed morphology and improve simulation/modelling. For some samples TEM can provide core size/ shape.	Statistically representative measurements can be time-consuming or impractical to obtain. Electron-induced damage of particles is a possibility.
Atomic force microscopy	Can provide topography, size measurement.	As with SEM/TEM, statistically significant measurements can be time-consuming
Dynamic light scattering (Solution based)	Can provide size of particles.	As a solution-based technique, measurements are not necessarily representative of samples under vacuum. Size measured is Stokes/hydrodynamic diameter.
Differential centrifugal sedimentation (Solution based)	Can provide high-resolution size distribution of particles, i.e. information on polydispersity.	As a solution-based technique, measurements are not necessarily representative of samples under vacuum. Can prove difficult for samples with density close to that of water. Size measured is Stokes/ hydrodynamic diameter.
Nanoparticle tracking analysis (Solution based)	Can provide size of particles.	As a solution-based technique, measurements are not necessarily representative of samples under vacuum. Size measured is Stokes/ hydrodynamic diameter.
Single-particle inductively-coupled-plasma mass-spectrometry	Can provide size distribution and elemental information.	Elemental information limited, minimum particle size detectable controlled by analyte sensitivity

Table 7 *(continued)*

Technique	Benefits	Disadvantages
Coating thickness measurement		
Other techniques can be used to corroborate measurements of coating thickness performed using electron spectroscopies		
Low-energy ion scattering	Can be used to provide measurements of overlayer thickness, and can identify the presences of uncoated core, i.e. pinholes, incomplete shell coverage[10],[120],[121].	Typically requires a high-Z core, low-Z shell.
Transmission electron microscopy (TEM)	Can be used to determine size and coating thickness for nanoparticles with distinct contrast between the coating and the core.	Statistically representative measurements are time-consuming to obtain. Electron-induced damage of particles is a possibility.
Any size determination technique performed separately on cores and complete particles	As simple to perform as the technique chosen, many possible techniques are options (see 'size determination' section above).	Requires access to bare 'cores' without coating. Error can be influenced by differing behaviour of the cores compared to the coated particles with respect to certain techniques (e.g. in solution, some materials may have different hydrodynamic radii for the same 'dry' size; in electron microscopy, some materials may degrade under the electron beam). Core needs to be unchanged by coating process.
Structure and/or composition		
Structure and composition can aid in identifying sources of error and justifying assumptions made when estimating coating thicknesses		
Small angle X-ray/Neutron Scattering (SAXS/SANS) (Solution Based)	Can identify size and structure of a population of nanoparticles.	Requires complex modelling, particularly for non-ideal systems. Interpretation can be difficult without a reasonable initial understanding of the sample
Thermogravimetric analysis	Can provide material composition of a nanoparticle system.	Dependent on thermal breakdown of materials – unsuitable for materials with complex breakdown processes. Provides a 'bulk' view of composition – insensitive to location or structure of materials.
Scanning transmission X-Ray microscopy	Can provide information on size and shape of individual particles, image contrast based on chemical composition, less beam-induced damage than electron-beam-based methods.	Statistically representative measurements are time-consuming, X-ray-induced damage of particles is a possibility.
X-ray diffraction	Can provide info on crystal structure and potentially crystallite size for dry samples.	Sensitive to ordered structures – particles need to be randomly oriented to obtain useful information on crystal structure of the population. Only applicable to crystalline samples.
Energy dispersive X-ray analysis (EDX)	Can provide information on total elemental composition of the particle. Line scans can be used to determine coating thickness.	Statistically representative measurements are not practical. Electron-induced damage of particles is a possibility.

Table 7 *(continued)*

Technique	Benefits	Disadvantages
Medium-energy ion scattering	Can provide a range of useful information including size and elemental distribution of nanoparticles.	Complex structures can require careful modelling for data interpretation; can require careful sample preparation (monolayer of particles is preferable)

9 Deviations from ideality

9.1 General

The majority of nanoparticle systems do not conform to the idealised model of a monodisperse population of particles with a uniform, homogeneous core and a similarly uniform concentric coating. Depending on the particular deviation, the coating thickness estimation methods described previously could potentially still provide useful information, either with some additional calculations, or simply with some qualification. In practical application, often such non-ideal systems can in fact contain a mixture of several deviations from the idealised model. In such cases, the analysis may prove difficult, and there may be no single, unique solution. Any analysis provided by modelling or calculation in such a scenario needs to take this into consideration, and ideally include corroboration from complementary techniques.

9.2 Multilayered coatings

The specific case of multi-layered coatings, particularly 2-layer or "core-shell-shell" particles is of great interest to industry, with many such particles now commercially used[122]–[125]. In general, systems in which an additional overlayer is present on top of a 'core-shell' particle cannot be easily analysed, as the range of potential morphologies that can give rise to a given ratio of peak intensities increases significantly. Where other analytical techniques can be used to establish some parameters of the system, such as the concentricity of the coatings and particle diameter, reasonable analysis of electron spectroscopy data can be obtained. Such systems can then be reasonably easily modelled using numerical methods, and simulation software such as SESSA will typically be able to model such systems with ease. In cases where the coating layers are of similar materials, such multiple organic overlayers, the total combined thickness can be reasonably estimated using the T_{NP} formula mentioned previously. For systems in which this is not the case, or in cases where estimates for the thicknesses of both coating layers are desired, an extension of the T_{NP} method has been demonstrated which can be used to estimate the thickness of both overlayers. As with the T_{NP} method, the 'core-shell-shell', or *CSS-*T_{NP} method was developed by comparison and fitting to numerical modelling data generated using the method described previously.

In order to determine the thicknesses of two coating layers on a particle, this method initially considers two separate approximations (see Figure 15) and requires iteration between the two, typically converging within 2-3 cycles. For the purposes of calculating the outer-layer thickness, the core and inner shell are considered as a unified 'core', with their intensities weighted to account for the differing attenuation of signal between them. For the purposes of calculating the inner layer thickness the core and inner-layer are considered as a standard 'core-shell' system, with an adjustment applied to account for the attenuation of signal due to the outer shell. As with the original T_{NP} method, the *CSS-*T_{NP} method utilises the ratios of effective attenuation lengths to minimise the complexity of the resulting equation.

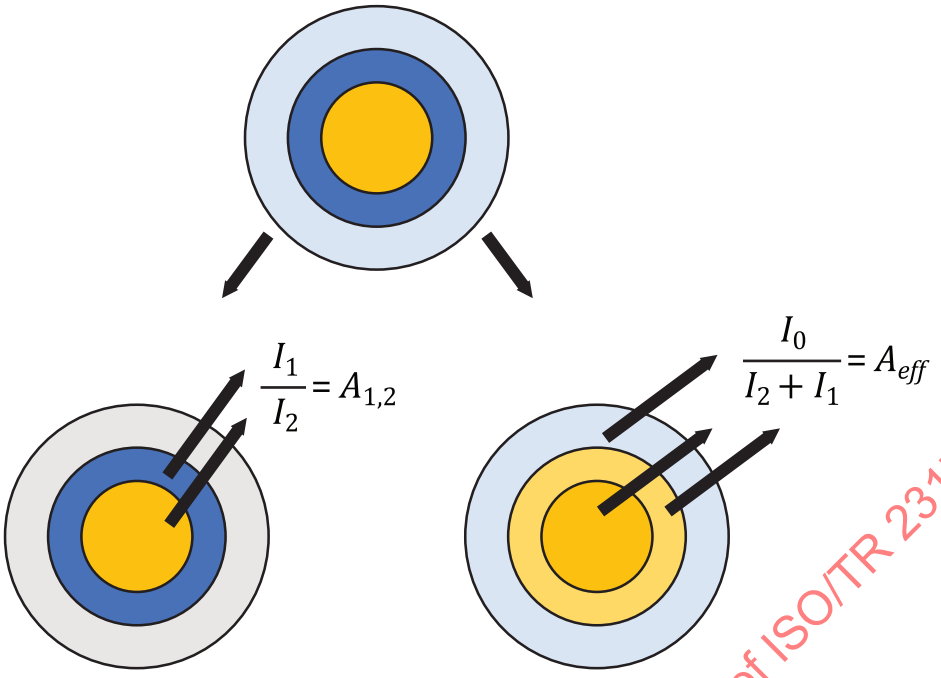

NOTE I_i indicates the intensity from a material; here, i= 0 denotes the outer coating layer, i=1 denotes the inner coating layer, and i=2 denotes the core.

Figure 15 — Schematic describing the two approximations utilised in the *CSS-*T_{NP} method

Once these ratios have been determined and starting with an estimate of either the inner or outer coating thickness, correction factors can be applied to the measured intensity ratios indicated in Figure 15 ($A_{1,2}$ and A_{eff}). These corrected intensity ratios can then be used as inputs within the standard T_{NP} formula to obtain thickness estimates for each layer. Iterating between calculating the inner and outer coating thicknesses results in convergence typically within 2 or 3 cycles, even with an initial estimate that is incorrect by an order of magnitude.

As this method is based upon the T_{NP} method, the primary sources of uncertainty are similar. Due to the use of the straight-line approximation in the modelling, cases with significant elastic scattering can introduce greater error. Figure 16 shows plots of the distribution of calculated overlayer thicknesses to modelled thicknesses for 5 000 randomly generated particles. It can be seen that there is more significant variability in the estimation of the inner shell thickness (T_1) than in the outer shell thickness (T_2), however for both these distributions the standard deviation is less than the 10 % uncertainty in estimation of the effective attenuation lengths[23].

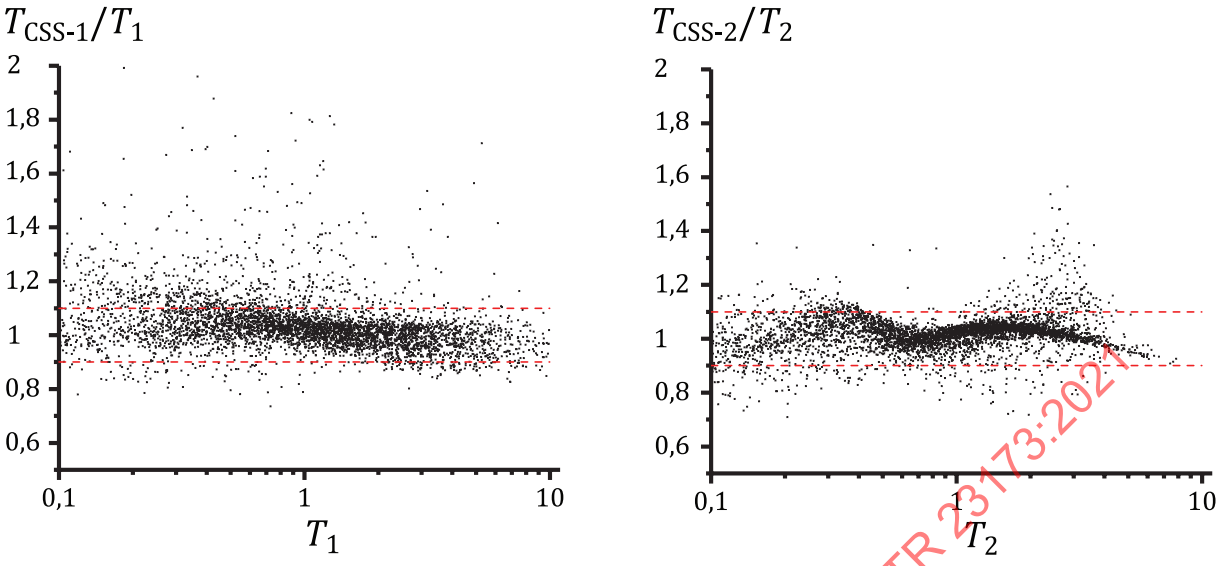

a) Inner coating layer **b) Outer coating layer**

NOTE Red dashed lines indicate 10 % deviation of the calculated value from the modelled value.

Figure 16 — Plots of the ratio of calculated to modelled thicknesses for both the inner coating layer and the outer coating layer

9.3 Other non-ideal cases

For nanoparticles possessing only a single coating layer, there remain a variety of possible deviations from the idealised model often assumed. These can relate to surface morphology, structure, or composition. In reality, no nanoparticle system is a perfect match to the ideal assumed case, so it is of value to understand how such variations from this case can manifest in a typical calculation of a coating thickness. As a general rule, most structural or morphological deviations that are unaccounted for when performing a coating thickness calculation will skew the calculation towards a lower thickness. This is due to the exponential nature of the attenuation of electrons; when averaging over a region in which there is variation in the observed overlayer thickness, the measured signal from the substrate (i.e. the core in the case of nanoparticles) will be greater than that that would arise from an equivalent average overlayer of uniform thickness (Figure 17).

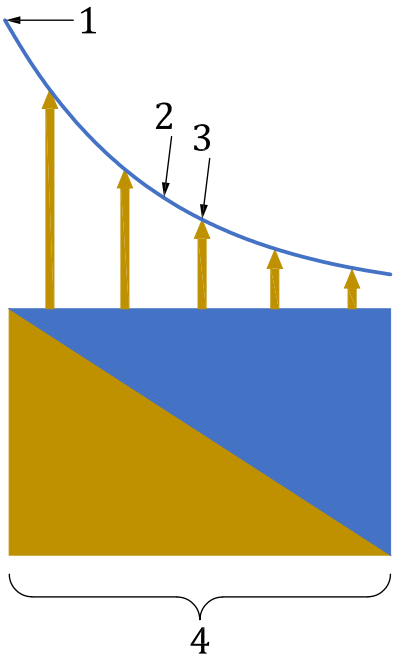

Key

1 pure material intensity
2 observed XPS intensity
3 average overlayer
4 sample depth beyond base of schematic significantly greater than effective attenuation lengths

NOTE Substrate material is considered to extend to a depth much greater than the relevant EAL.

Figure 17 — Schematic illustrating the difference between average overlayer thickness and the equivalent observed XPS intensity as a result of the exponential nature of electron attenuation

For compositional variations, the issue is more complex and, in some cases, the concept of an overlayer thickness can no longer be the most useful measurand, or even a reasonable quantity to define. This is particularly true of cases where the boundary between core and coating is not abrupt. For some structures, where the deviation from the ideal case is well understood, simulation software has been demonstrated to accurately model the resulting XPS spectrum[34]. Where such software is not available, any interpretation needs to be performed with care, and an understanding of the effects of any given structure on the measured intensities. Table 8, below, lists and illustrates some common potential deviations from the ideal case, with comments regarding how these can be considered. For conciseness, a nanoparticle system which meets all of the assumptions described previously (e.g. uniform homogeneous materials, concentric spherical core and coating, etc.) is referred to as an "ideal system".

Table 8 — Illustrated list of common deviations from an ideal concentric coated nanoparticle structure, alongside comments regarding their analysis

Deviation	Illustration	Comments
Non-uniform coating or core morphology; random roughening	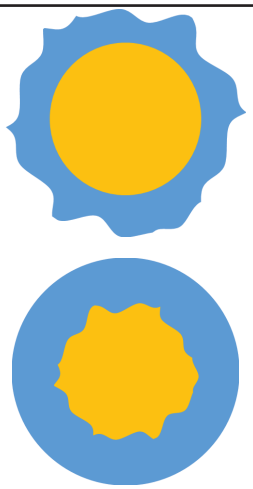	The observed spectrum for a system of this type will appear equivalent to that of an ideal system with an overlayer thinner than the real mean thickness. Cases with roughening or non-uniformity in the coating which has a directional bias can be considered as asymmetric or non-concentric coatings.
Polydispersity in core or coating size	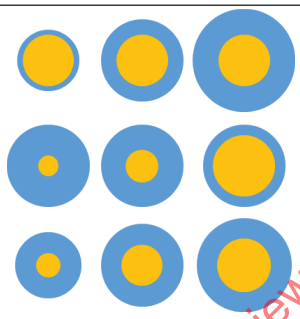	The effect of moderate polydispersity in a normal distribution will not be significant for most systems. In particular, polydispersity in core size, with a monodisperse coating thickness will have very little effect for all but very small nanoparticles. Where there is significant polydispersity in coating thickness, estimated coating thicknesses will appear equivalent to that of a monodisperse system with an overlayer thinner than the real mean thickness.
Incomplete coating	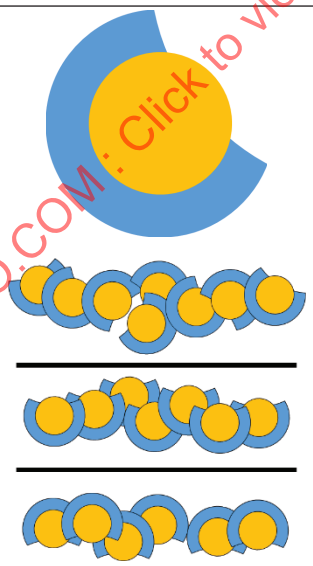	The observed peak intensity for a system with an incomplete coating, where particles are randomly oriented with respect to the coating, will appear equivalent to an ideal system with a thinner coating. In some cases, this scenario can be identified by visual inspection of the inelastic background. In cases where the orientation with respect to the coating is fixed, this can result in an even thinner estimate for the coating (if the coating gap is universally 'face-up'), or can appear similar to the equivalent ideal case (if the coating gap is universally 'face-down')

Table 8 *(continued)*

Deviation	Illustration	Comments
Non-concentric coating	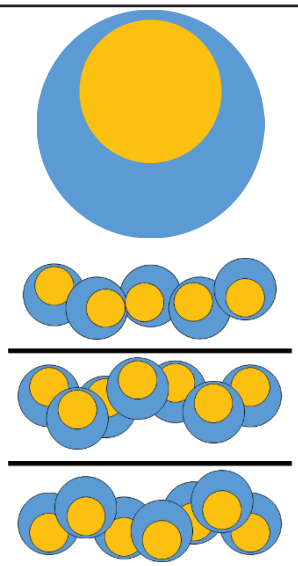	The observed spectrum for a system with a non-concentric coating in which particles are randomly oriented will appear equivalent to an ideal system with a thinner coating layer. If the nanoparticles are ordered with respect to the core position, the effect will depend strongly on this orientation – a bias towards the point of minimum vertical coating thickness (i.e. the line from the core to the detector which passes through the least material) will be present in calculations of overlayer thickness if this effect is not compensated for.
Asymmetry of core or coating	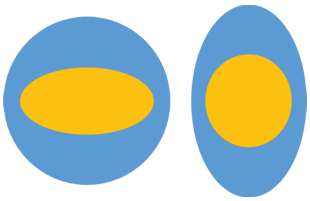	Asymmetry of the core or coating on a nanoparticle will have a similar, but more pronounced effect to that of a non-concentric coating. As with a non-concentric coating, there will always be an orientation in which the coating thickness observed is at a maximum. As such, for randomly oriented particles, a bias towards the minimum observed coating thickness will be observed when calculating overlayer thicknesses if this effect is not accounted for. For ordered particles, the thickness estimated will instead be dominated by the side facing the detector.
Non-abrupt boundaries – core/coating mixing at interface	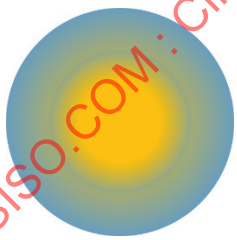	The concept of coating thickness becomes ill-defined for systems in which the boundary between core and coating materials cannot be reasonably approximated as an abrupt interface. Calculations of coating thickness which assume an ideal system will be skewed towards a value that is thinner than the median point for a linear mixing gradient; for more complex scenarios the effect will not be so clearly definable. Calculated coating thicknesses could reasonably provide useful comparative information with respect to similar systems, but a more explicit interpretation is not justifiable without detailed modelling.
Non-homogeneous density of coating or core	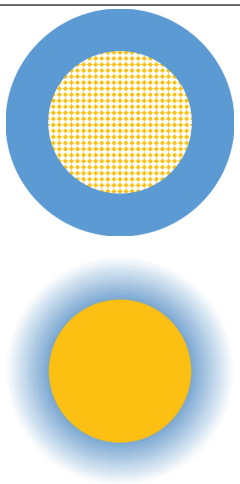	In systems where there is minor variation in core density, the effect will rarely be significant, and is not dissimilar to an equivalent reduction or increase in core size, excluding the effect on curvature. In systems with a variation in coating density, such as with organic molecules bound to the core, it is more reasonable to consider the coating thickness estimate to correspond to an amount of material present rather than an actual thickness (which will typically vary depending on environment for such systems). In this case, such estimates remain useful, but care needs to be taken to ensure the interpretation is conveyed as a comparative quantity rather than a literal thickness.